



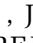







Cool deltas: Sedimentological, geomorphological and geophysical characterization of ice-contact deltas and implications for their reservoir properties (Salpausselkä, Finland)

BARTOSZ KURJAŃSKI* , BRICE R. REA* , MATTEO SPAGNOLO* ,
DAVID G. CORNWELL* , JOHN HOWELL* , JEAN-CHRISTOPHE COMTE* ,
ANDRÉS GONZÁLEZ QUIRÓS* , JUKKA-PEKKA PALMU† , RACHEL P. OIEN* 
and PHILIP L. GIBBARD‡ 

*School of Geosciences, University of Aberdeen, King's College, Aberdeen, AB24 3FX, UK
(E-mail: bkurjanski@abdn.ac.uk)

†Geological Survey of Finland (GTK), Vuorimiehentie 5 P.O. Box 96 FI-02151, Espoo, Finland

‡Scott Polar Research Institute, University of Cambridge, Lensfield Road, Cambridge, CB2 1ER, UK

Associate Editor – Victoria Valdez

ABSTRACT

Sediments deposited by glacial meltwaters (for example, ice-contact delta deposits) form permeable packages in the subsurface that can act as reservoirs for both water and hydrocarbons. They are also an important source of aggregate for the construction industry. As reservoirs they are challenging to characterize in terms of their structure, flow and storage properties due to their complex depositional history. In this study, ice-contact deltas of Salpausselkä I and II end moraines in Southern Finland are studied using a combination of geomorphological mapping, sedimentological studies and near surface geophysical methods. Sedimentary logs from isolated outcrops were correlated to ground penetrating radar (GPR) profiles to unravel the internal structure and depositional history of these ice-contact deltas. Subsequently, electrical resistivity tomography (ERT) and gravity data were analysed to estimate the depth to bedrock and to model porosity distribution within the sediments. Results of the study suggest that the delta deposits have a broad range of porosities (10 to 42%) with lowest values found in the bottomset beds. The most variable porosities are in the subaqueous ice-contact–fan zone, and consistently high porosities occur in delta foreset/topset facies. Detailed sedimentary logging linked to the GPR data shows heterogeneities such as mud drapes on foresets and kettle holes which are below the resolution of ERT and gravity methods but significantly affect reservoir properties of the deltas. Moreover, oscillation of the ice-margin may have introduced larger heterogeneities (for example, buried ice marginal ridges, or eskers) into the sedimentary sequence which are atypical for other Gilbert-type deltas. Finally, subglacially sculpted, highly variable bedrock topography exerts a major control on sediment distribution within the delta making reservoir volume and quality less predictable. This work has implications for present-day freshwater aquifers and low enthalpy geothermal energy in southern Finland and other deglaciated regions, as well as hydrocarbon exploration of analogous deposits in the subsurface from Pleistocene and pre-Pleistocene glaciogenic sequences.

Keywords Finland, glaciogenic sediments, ground penetrating radar, ice-contact deltas, reservoir properties, Younger Dryas.

INTRODUCTION

Sands and gravels deposited by glacial meltwater are the most exploited of all glaciogenic sediments as aquifers (Gabriel *et al.*, 2003; Maries *et al.*, 2017; Ravier & Buoncristiani, 2017; Erickson *et al.*, 2019), source of aggregate for the construction industry (Fisher & Smith, 1993; Levson *et al.*, 2003; Mossa & James, 2013; Bendixen *et al.*, 2017, 2019) or hydrocarbon reservoirs (Hirst *et al.*, 2002; Osterloff *et al.*, 2004b; Huuse *et al.*, 2012; Ottesen *et al.*, 2012; Rose *et al.*, 2016). Significant accumulations of well-sorted sands and gravels are often linked to the stabilization of retreating ice margins allowing meltwater to deposit, and accumulate, sediment proximal to the ice margin as sandar, ice-contact fans or deltas (Lønne, 1995; Zieliński & Loon, 1998, 1999, 2000; Saarnisto & Saarinen, 2001; Russell & Arnott, 2003; Zielinski & Loon, 2003; Thomas & Chiverrell, 2006; Winsemann *et al.*, 2009, 2018; Benn & Evans, 2010; Gruszka *et al.*, 2012; Hirst, 2012; Lang *et al.*, 2012, 2017b; Pisarska-Jamroz & Zieliński, 2014; Dietrich *et al.*, 2017a). Reservoir and aquifer properties at the intra-borehole/well scale are a function of the sedimentary architecture, which at present is poorly understood in ice-margin systems. These are also commonly more complex than other clastic systems because they are heavily influenced by rapid oscillations of the ice-margin and high variability of meltwater energy resulting in deposition of sediments by a combination of supercritical and subcritical flows. Recently, sedimentary structures associated with supercritical flow have been recognized from outcrops of proglacial braid plains, fans and deltas but also in non-glacial environments (Russell & Arnott, 2003; Dietrich *et al.*, 2016; Winsemann *et al.*, 2016; Covault *et al.*, 2017; Lang *et al.*, 2017a, 2021; Hage *et al.*, 2018; Winsemann *et al.*, 2018; Kostic *et al.*, 2019; Lin & Bhattacharya, 2020) and criteria for their recognition in glaciogenic sequences are being developed (e.g. Alexander *et al.*, 2001; Ghienne *et al.*, 2021; Lang *et al.*, 2021).

Unconsolidated, Pleistocene and Holocene glaciogenic sediments are especially important as aquifers in regions where repeated episodes of subglacial erosion have removed the older, pre-Pleistocene porous, sedimentary cover, leaving only impermeable crystalline basement across much of the area (Knutsson, 2008; Comte *et al.*, 2012; Ravier & Buoncristiani, 2017). In

such places, glaciogenic sands and gravels are often the only viable aquifers for human consumption, agriculture and industry. Understanding their distribution and internal structure is crucial for effective groundwater extraction and also for protection and management (Anderson, 1989; Poeter & Gaylord, 1990; Heinz *et al.*, 2003; Slomka & Eyles, 2013; Best *et al.*, 2015; Erickson *et al.*, 2019; Ó Dochartaigh *et al.*, 2019). Glaciogenic sediments also act as hydrocarbon reservoirs in areas such as the North Sea (Huuse *et al.*, 2012) and across North Africa (e.g. Osterloff *et al.*, 2004a; Slomka & Eyles, 2013; Kurjański *et al.*, 2020). The ability to predict physical properties of such sediments largely depends on understanding the depositional processes responsible for their formation (Lønne, 1995; Zieliński & van Loon, 2000; Heinz *et al.*, 2003; Catuneanu, 2006; Hirst, 2012; Slomka & Eyles, 2013; Zecchin *et al.*, 2015; Dietrich *et al.*, 2017a; Winsemann *et al.*, 2018; Lang *et al.*, 2021). This information is typically obtained by detailed sedimentological studies of wells and/or outcrop analogues (Howell *et al.*, 2008). Given that wells and many outcrops are spatially limited and two-dimensional it can be difficult to extrapolate results over a wider area especially given the heterogeneity of glaciogenic sequences (Hirst *et al.*, 2002; Lajeunesse & Allard, 2002; Reinardy & Lukas, 2009; Evans *et al.*, 2012). Shallow geophysical methods can be used to bridge that gap and provide missing information between wells or exposures, but are labour-intensive and costly. Moreover, seismic resolution decreases with depth thus affecting the imaging of deeply buried sediments (Andersen *et al.*, 2012; Ottesen *et al.*, 2012; Rose *et al.*, 2016; Battler *et al.*, 2019). S-wave seismic with a land-streamer system can be helpful because it enables fast acquisition of data and can provide high-resolution images of the near subsurface (Brandes *et al.*, 2011; Winsemann *et al.*, 2011, 2018). On the other hand, aquifer studies often rely heavily on near surface geophysical methods which are characterized either by high resolution and shallow penetration depth (for example, ground penetrating radar) or deeper penetration with lower resolution (for example, electrical resistivity tomography, seismic refraction and gravity), only imaging large contrasts in physical properties and discontinuities. Careful consideration is needed when choosing methods to deploy, ideally allowing identification of key heterogeneities (Gabriel *et al.*, 2003; Andersen *et al.*,

2012; Galazoulas *et al.*, 2015; Paz *et al.*, 2017; Ravier & Buoncristiani, 2017).

The use of modern analogues is a standard practice in evaluations of ancient sedimentary successions (Galloway, 1975; Orton & Reading, 1993; Pye & Lancaster, 1993; Pye, 1993; Hartley *et al.*, 2010; Nyberg & Howell, 2016). This approach is justified when evaluating clastic marine, fluvial or aeolian successions, since their scale and formation processes, with some exceptions, are reasonably similar across geological time. However, it may not be ideal when analysing glaciogenic deposits associated with continental-scale ice sheets, because of the different spatial and temporal scales of the processes involved. Parallels between modern and ancient glacial systems can still be useful, but the differences of scale and magnitude of observed processes have to be taken into consideration (e.g. Spedding & Evans, 2002; Evans, 2006; Evans *et al.*, 2009, 2017; Slomka & Eyles, 2015; Lee *et al.*, 2018). The best approach to understanding deep-time, ice-sheet derived sediments is to study glaciogenic deposits remaining on the land surface following the deglaciation of a region (Dietrich *et al.*, 2018; Dowdeswell *et al.*, 2019). Especially valuable study areas are those located where an ice-sheet margin was grounded in water and which are, today, above sea level; of these, the Salpausselkä I and II are excellent examples.

In this study a series of ice-contact deltas that constitute part of the Salpausselkä I and II end moraines in southern Finland, were investigated. The deltas are important aquifers and sources of aggregate for the region. Geomorphological mapping and sedimentological studies were integrated with a suite of near-surface geophysical methods [ground penetrating radar (GPR), electrical resistivity tomography (ERT) and gravity] to identify the sedimentary architecture, key heterogeneities, and provide insights into the formation and reservoir properties. Results of this study are applicable to groundwater reserve estimation and management in glaciofluvial deposits of southern Finland, but also to water and hydrocarbon exploration in glaciogenic sequences in general.

STUDY AREA

The Younger Dryas stadial (YD), a period of rapid climate cooling, occurred between 12.9 and 11.5 [cal kyr BP] (Walker *et al.*, 2009).

Retreat of ice masses from the Last Glacial Maximum (26.5 to 20 years ago [cal kyr BP] – e.g. Ehlers *et al.*, 2011; Hughes & Gibbard, 2015) was paused and in some instances reversed (Demidov *et al.*, 2006; Kalm, 2012; Marks, 2012; Carlson, 2013; Stroeven *et al.*, 2016; Patton *et al.*, 2017).

In southern Finland, the Younger Dryas Stadial stillstand/re-advance of the Fennoscandian Ice Sheet (FIS) is represented by three large (hundreds of kilometres long) moraine ridges Salpausselkä I, II and III (oldest to youngest, respectively) (Fig. 1). The moraine ridges are constructed predominantly of meltwater-transported material, deposited very rapidly (200 to 250 years) in the ice-marginal depositional zone (Kurjanski *et al.*, 2020) as a system of coalescing ice-contact deltas, subaqueous fans and composite ridges when the FIS was grounded in the Baltic ice lake (Sauramo, 1929, 1931; Donner, 1969, 1995, 2010; Glückert, 1986, 1995; Fyfe, 1990; Saarnisto & Saarinen, 2001; Rinterknecht *et al.*, 2004; Lunkka *et al.*, 2020).

The study area is the Lahti region, Finland, which was at the confluence zone between the Baltic and Finnish Lake District ice lobes during the YD Stadial (Fig. 1). Four outcrops of Salpausselkä I were visited and studied in active gravel pits located in Kukonkangas, 15 km west of Lahti (Fig. 2, locations 1 to 4). Two further Salpausselkä I localities were studied in the area known as Hälvälänkangas, 15 km WNW of Lahti (Fig. 2, locations 5 and 6). Salpausselkä II was studied from sites located near Vierumäki, 20 km NNE of Lahti (Fig. 2, locations 8 to 13). The data were collected from the Syrjälänkangas (GPR, ERT and outcrop), Hyrtiälänkangas (GPR and ERT), Vesivehmaankangas (GPR and ERT) and Mikkolänkangas (outcrop and GPR) areas (Fig. 2).

Geology and morphology of the study area

The bedrock geology is dominated by crystalline rocks of the Fennoscandian Shield formed, or metamorphosed, during the Svecofennian Orogeny, 1.92 to 1.77 Ga (Paulamäki *et al.*, 2002; Nironen, 2017). In the Lahti region granite, microcline granite, quartzite, gabbro and paragneiss are dominant (Nironen, 2017). Late Cenozoic glaciations are responsible for the removal of pre-Pleistocene strata and sculpting of the crystalline bedrock surface (Figs 1 to 3).

The sedimentary cover is thin, ranging between 0 to 30 m with the exception of the Salpausselkä I and Salpausselkä II ridges, where

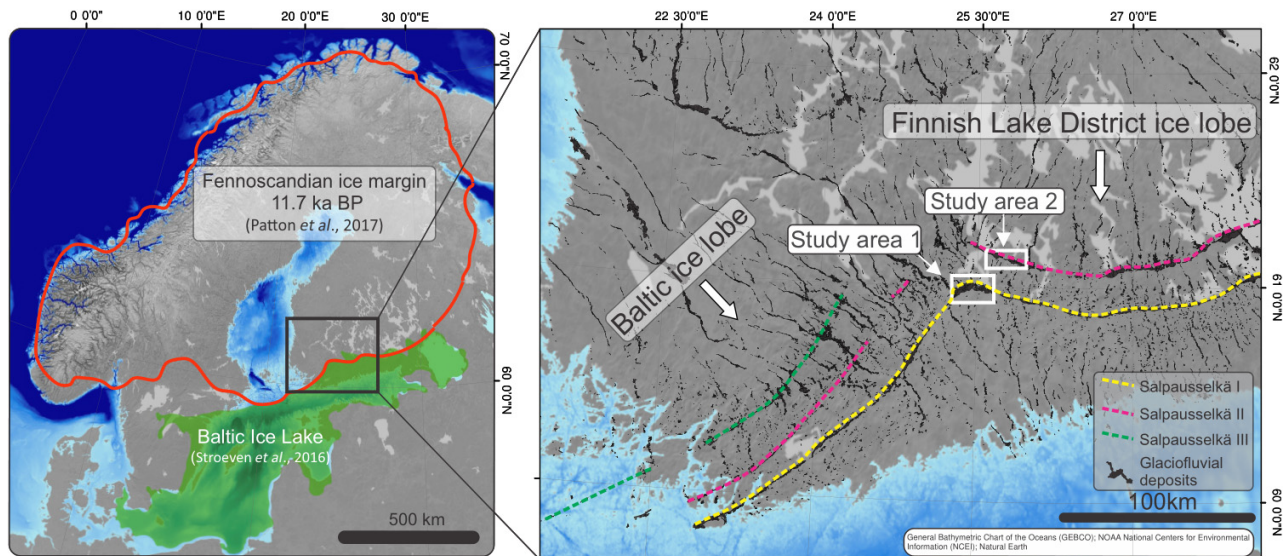


Fig. 1. Location of the study area in Finland. Left: approximate extent of the Fennoscandian Ice sheet and Baltic ice lake at the time of deposition of Salpausselkä ridges. Right: map of surficial glaciofluvial deposits in southern Finland with ice-margin positions marked (Salpausselkä I–III). Glaciofluvial deposits trending north–south (NE–SW and NW–SE) delineate subglacial meltwater conduit networks (eskers) beneath the Fennoscandian ice sheet. White arrows indicate approximate ice flow direction during the Younger Dryas Stadial.

thicknesses often exceed 50 m (Fyfe, 1990; Palmu, 1999; Johansson *et al.*, 2011). The Salpausselkä I and Salpausselkä II deposits are stratigraphically higher than the underlying till and sand (Figs 1 and 2).

METHODOLOGY

This study combines outcrop analyses, and acquisition, processing and interpretation of ground penetrating radar (GPR) and electrical resistivity tomography (ERT) data. These were analysed jointly and interpreted in combination with pre-existing Light Detection and Ranging (LiDaR) Digital Elevation Model (DEM) and gravity (Bouguer anomaly) data, to provide information on the depositional processes, sedimentary environments, reservoir geometries and properties of the ice-contact deltas. Additional metrics and reservoir properties were calculated.

Geomorphology

A LiDaR DEM (1 m horizontal resolution and 0.3 m vertical resolution) (Fig. 2), provided

courtesy of the National Land Survey of Finland and processed by the Geological Survey of Finland, was used to map and analyse the morphology of the study area (Figs 2 and 3). Mapping was conducted using ArcGIS®. The landforms were mapped based on their expression in the DEM, overlain with a 75% transparent multidirectional hill shaded raster, and a 75% transparent slope raster, to best highlight the morphological features. Morphometrics and topographic profiles were also extracted using ArcGIS (Fig. 2).

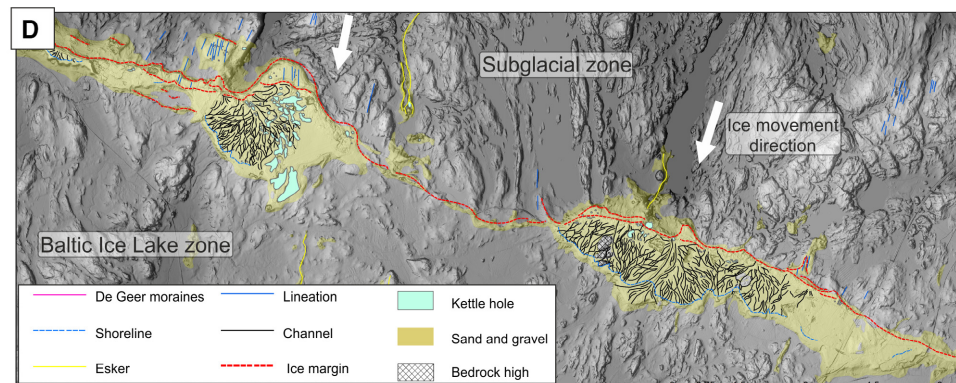
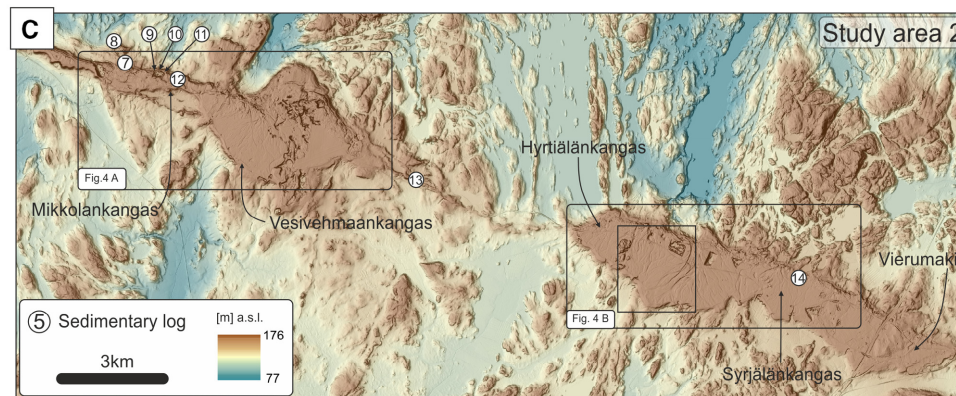
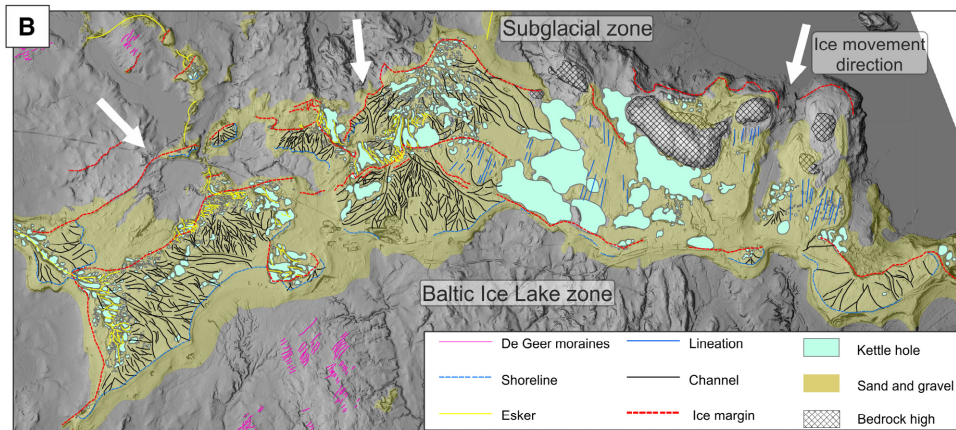
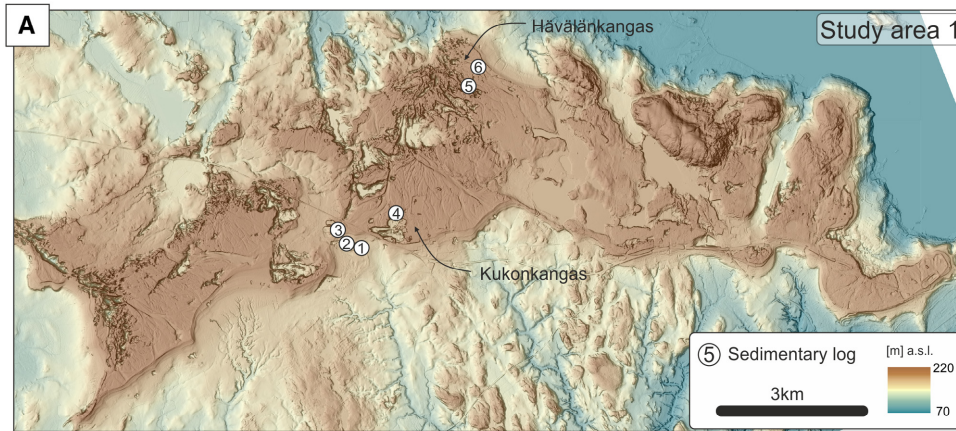
Sedimentology

Fourteen outcrop sections, ranging between 4.5 to 23 m in height, were logged in detail, up to the decimetre scale, where possible, in active gravel workings. Five sections were located in Salpausselkä I (Fig. 2A), whilst two further gravel pits in Salpausselkä II were studied (Fig. 2C).

Ground penetrating radar

The GPR profiles were acquired in the Vierumäki region in Salpausselkä II (Fig. 3). Fifteen

Fig. 2. The digital elevation model of the study area (A) and (C) and the geomorphology (B) and (D). In (A) and (C) numbers indicate the locations of the sedimentary logs (see Fig. 6).



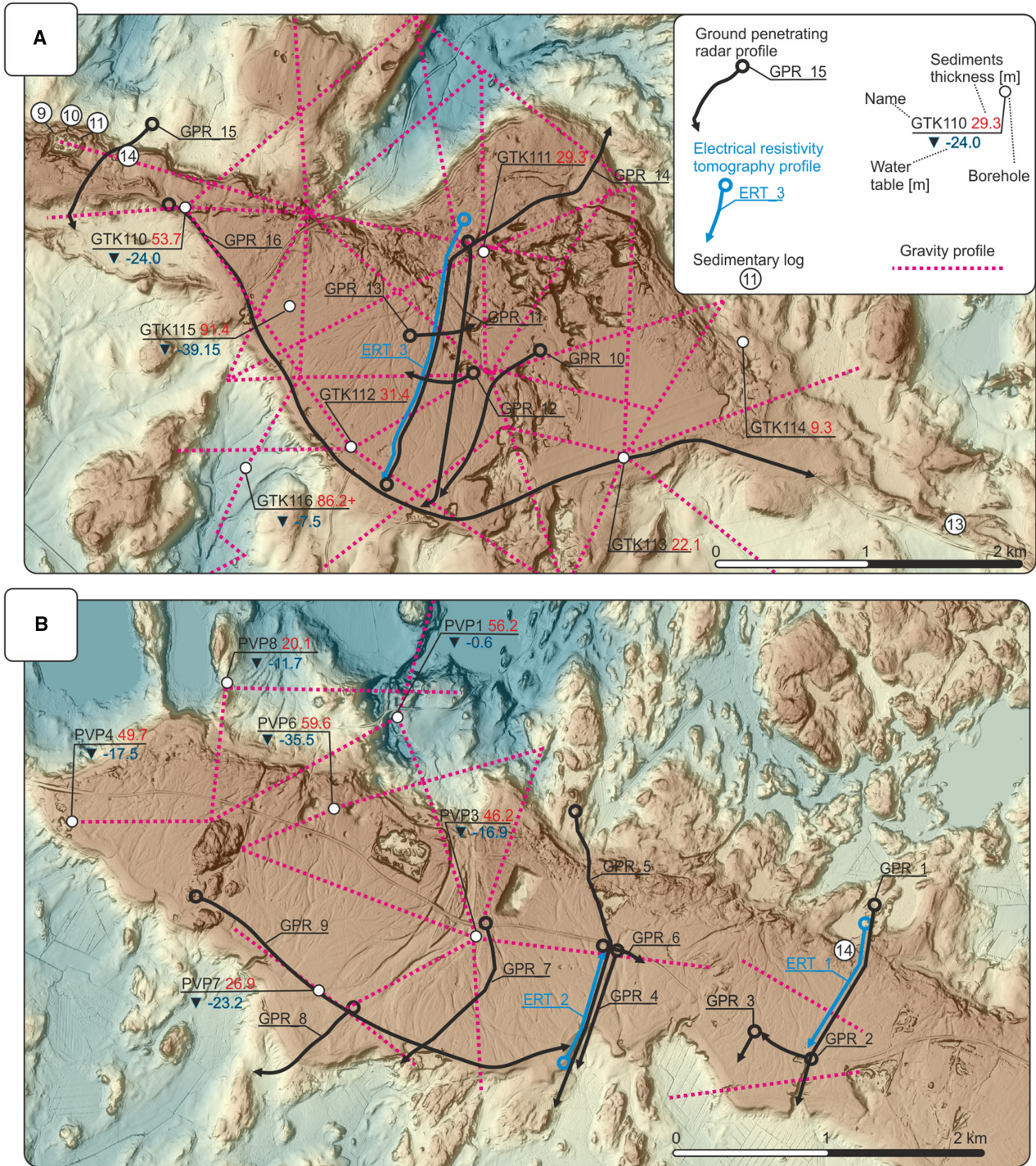


Fig. 3. Map showing the locations of the geophysical measurements and data available over the study area 2: (A) Vesivehmaankangas; and (B) Hyrtiälänkangas localities.

80 MHz GPR profiles (14 km) were acquired with a horizontal resolution of 11 cm and a vertical resolution estimated to be 0.2 to 0.6 m, depending on the dielectric properties of the material. The penetration depth is between 5 to

25 m. GPR profiles were collected along existing forest roads, as close as possible to the depositional dip and strike directions (Fig. 3). In some locations, where outcrops were close to the survey line, it was possible to directly correlate

GPR results with lithologies and sedimentary structures observed in the outcrop (Fig. 3). For equipment and processing details see Table S1.

Electrical resistivity tomography

The ERT survey (Fig. 3) was undertaken to determine the depth to bedrock and to correlate resistivity zones with the reflection packages identified using the GPR and, in turn, link to the sedimentary facies, to better understand the sedimentary architecture at depth. Three ERT profiles were acquired across the study area (Fig. 3): ERT1 (1075 m length); ERT2 (720 m); and ERT3 (1875 m), in a north–south orientation (parallel to the depositional dip) and co-linear with GPR profiles GPR 1, GPR 4 and GPR 14, respectively (Fig. 3). Dipole–dipole (DD) and multigradient (mGD) quadripole arrays were used jointly to ensure optimum resolution for imaging the complex arrangement of glacial sediments overlying fractured bedrock (Comte *et al.*, 2012). The depth of investigation (DOI) method (Oldenburg & Li, 1999) was further applied to determine the maximum reliable depth of investigation. For equipment and processing details see Table S1.

Porosity from ERT

The porosity of the individual zones was calculated based on Archie's Law (Eq. 1) which relates pore fluid conductivity (C_t) with the resistivity of the bulk volume (R_t) (Eq. 2) (Archie, 1942):

$$C_t = \frac{1}{\alpha} C_w \phi^m S_w^n \quad (1)$$

$$R_t = \frac{1}{C_t} \quad (2)$$

where: ϕ is porosity (0 to 1), R_t is resistivity from ERT profiles [Ωm], C_w is conductivity of formation waters [S/m], C_t is conductivity of bulk rock [S/m], S_w is water saturation (0 to 1), n is water saturation exponent and m is cementation factor. Tortuosity factor – α is unknown and was assumed to be unity (1) to enable comparison between results. Combining Eqs 1 and 2 allows porosity ($\phi = 0$ to 1) to be calculated. This method was chosen because it is suitable for clay-poor formations of Salpausselakäs (Okko, 1962; Glückert, 1986; Fyfe, 1990; Palmu, 1999).

Parameters used for porosity calculation from ERT profiles are listed in Table 3. They were

modelled using a Monte Carlo simulation based on a normal distribution of parameters. Input parameters (mean and standard deviation) were calculated based on available literature (see Tables 1 and 2 for details). Water saturation values were determined based on boundary conditions: dry and saturated sediments should have similar porosity values and the resistivity response is mainly governed by water saturation since the sediments within deltaic foresets are well-sorted and uniform. The results were validated by substituting calculated porosity values with average porosities of glaciofluvial sediments sourced from the literature and comparing the resulting resistivity values with resistivity recorded in the field.

Gravity and shallow borehole data

Gravity survey and borehole data, in a series of groundwater investigation reports, were available from the Geological Survey of Finland data repository, (www.hakku.fi; Fig. 3) (Breilin *et al.*, 2005, 2006; Ahonen *et al.*, 2011). Bouguer anomaly data were sampled approximately every 20 m along profiles (Fig. 3). Final interpretations (after inversion) of gravity profiles as well as published depth-to-basement maps were used to supplement interpretation.

MORPHOLOGY OF GLACIAL LANDFORMS

Ice-contact deltas

A series of flat-topped hills are present in the study area (Fig. 2). Their orientation is transverse to the ice flow during the Younger Dryas Stadial (Fig. 1). The ridges can be subdivided into lobate or irregular segments which, in places, amalgamate forming a broad plateau (Fig. 2). Eighty-six segments, 600 m to 19 800 m long (mean 4040 m, median 2830 m) and 190 to 7500 m wide (mean 1490 m, median 1020 m), were identified. Their height varies between the northern, ice-proximal side (55 to 65 m above the neighbouring topography) and the southern, ice-distal, side (45 to 50 m), but can reach up to 100 m near Aurinkovuori (N61.190159, E25.477587). The slope of the ice-proximal side ranges between 8.5° and 21.0° (mean 13.1°, median 12.2°) and is steeper than the ice-distal side (0.1° to 29.0°, mean 6.5°, median 4.8°). Plateau surfaces slope towards the south between 0.1°

Table 1. Sedimentary facies as identified in studied outcrops. For visual reference see Fig. S1.

Facies	Code	Grain size	Sorting	Sedimentary structures
Basal contact				
Diamicton	Dm All	Poor/very poor	Rafts and lenses of sands and gravels with preserved primary bedding/laminations, fold structures, reverse faults, secondary foliation, rotational structures, lenses of sands/gravels, oversized clasts	Erosional
Massive and crudely bedded boulder-cobble gravel	Cmb	Moderate/poor	Imbrication, planar bedding, large-scale cross-bedding	Erosional
Cross-bedded boulder-cobble gravel	Cx	Moderate	Imbrication, planar cross-bedding, trough cross-bedding, horizontal bedding	Erosional
Horizontally bedded boulder-cobble gravel	Ch	Good/moderate	Horizontal bedding, outsized clasts, boulder pavements, imbrication, sand and gravel lenses	Erosional
Massive and crudely bedded gravel	Gm	Good/moderate	Crude imbrication, outsized clasts	Erosional
Cross-bedded gravel	Gx	Good/moderate	Cross-bedding, scour-and-fill structures, outsized clasts	Erosional/conformable
Horizontally bedded gravel	Gh	Good/moderate	Outsized clasts, scour-and-fill structures, imbrication	Erosional
Trough cross-bedded sands	Stx	Good	Gravel lags, gravel lenses, winnowed gravel pavements, scour and fill structures	Erosional
Planar bedded sands	Sp	Good	Gravel lags/horizons, large-scale (foreset) cross-bedding	Conformable
Planar cross-bedded sands	Sp _x	Good	Planar cross-bedding, gravel horizons, gravel lenses, gravel pavements	Erosional/conformable

Table 1. (continued)

Facies	Code	Grain size	Sorting	Sedimentary structures
Basal contact				
Large-scale tangential cross-bedded sands	Stl	Coarse-medium sands, subordinate gravels	Gravel horizons, outsized clasts, dropstones	Conformable/erosional
Ripple laminated sands	Sr	Medium-fine sands	2D/3D current ripples, dropstones	Conformable
Climbing-ripple laminated sands	Scr	Fine-medium sands, subordinate silts	Climbing ripples, biotite plates accumulating on lee sides of the ripples	Conformable
Draping and planar laminated sands and silts	SFd	Fine sands and silts	Draping lamination grading upward to horizontal laminations, dropstones	Conformable/gradational
Draping and planar laminated silts and clays	Fd	Silts and clays	Draping laminations, planar laminations, dropstones	Conformable
Contorted clays, silts and sands	SFc	Clays-silts-fine to coarse sands, subordinate gravels	Soft sediment deformations, sand injections, load structures, ball-and-pillow structures	Loaded

and 2.8° (mean 0.4°, median 0.3°). The distal margin of the plateau is often characterized by a rim of sediment with several major breaks of slope (terraces) below and multiple intermediate, smaller slope breaks. The rim is interpreted as a shoreline delineating the level of the Baltic ice lake to which the delta aggraded, i.e. the emergent delta (top) surface (Fig. 2) (Glückert, 1995). Subsequent slope breaks are interpreted to represent wave erosion with shorelines forming as a result of the interplay between isostatic rebound and lake-level fluctuations (Jantunen & Donner, 1996; Eronen *et al.*, 2001).

Braided channels

The top surfaces of ice-contact deltas are often undulating, exhibiting a radial, braided pattern of furrows which are largely discontinuous and rarely extend the full breadth of the plateau (Fig. 2). Instead, they cross-cut or merge, creating a radial, dendritic pattern originating from an apex in the elevated, proximal part of the plateau. Multiple dendritic patterns can be observed on larger plateaus. Individual furrows can be traced for 8 to 2150 m (mean 148 m, median 222 m). They are 2 to 110 m wide (mean 50 m, median 35.5 m) and 0.2 to 10 m deep (mean 1.7 m, median 0.9 m) and interpreted to represent a distributary network of braided, channels preserved on emergent delta tops (Donner, 1976).

Kettle holes

Oval and irregular depressions are visible on the delta tops and some eskers (Fig. 2). The area of the depressions ranges between 36 m² and 1 042 300 m² (median 1428 m²). Individual depressions are 1 to 50 m deep (median 8 m). They are more abundant in the ice-proximal zones. Braided meltwater channels on delta tops can be on both sides of many depressions, which implies that the formation of depressions post-dates the delta formation. The depressions are interpreted as kettle holes formed from melt-out of buried or detached ice blocks (e.g. Wingfield, 1990; Palmu, 1999; Mäkinen & Palmu, 2008; Maries *et al.*, 2017). The size distribution of kettle holes allows division into three categories. (1) The largest kettle holes occur in the south-east part of Salpausselkä I delta complex, near Lahti (Fig. 2A). They are positioned in the leeside of a local bedrock high and potentially represent large dead ice blocks that became detached as the ice margin thinned and retreated over the bedrock high. (2) Large, deep and elongated depressions

exhibiting a linear or radial pattern (Fig. 2) are located mainly in the proximal, ice-contact parts of the hills, most likely representing dead ice blocks cut off from the ice margin by meltwater flow. (3) Small oval and irregular shaped, shallow kettle holes were likely formed by melt out of glaciofluvially deposited ice blocks, based on their distribution in the medial/distal part of the delta (Fig. 2).

Push moraines

Discontinuous, curvilinear or straight ridges are present locally on the proximal slope break. They range between 2 to 7 m (mean 3 m) in height above the top of the plateau and are 20 to 150 m wide (median 42 m, mean 55 m). They are interpreted as push moraines linked to ice-marginal oscillations (Aber *et al.*, 1989; Bennett, 2001; Benn & Evans, 2010). Where such oscillations were more substantial, ice overrode the proximal slope of the deltas and push moraines were on the delta top. (Fig. 2).

Interpretation

Based on the morphologies of the flat-topped hills and associated secondary landforms, the hills were interpreted as ice-contact Gilbert-type deltas deposited in a lake with water depths of 35 to 60 m above the present-day land surface (Gilbert, 1885, 1890; Glückert, 1986; Lønne, 1995; Palmu, 1999; Saarnisto & Saarinen, 2001; Thomas & Chiverrell, 2006; Dietrich *et al.*, 2017b; Kurjanski *et al.*, 2020). Meltwater and sediments were supplied to the ice margin chiefly via subglacial/englacial meltwater channels and deposited under water, proximal to the grounding line as ice-contact, subaqueous fans (Powell, 1990). The sediment supply was sufficiently great that fans aggraded to the contemporaneous water surface resulting in ice-contact delta formation and subsequent progradation. Following delta emergence, the sediments were transported in sub-aerially fluvial channels across the delta-top (topset facies) and were deposited on as sub-aqueous foresets and bottomsets (Gobo *et al.*, 2015; Dietrich *et al.*, 2017b; Lang *et al.*, 2017b). Sediment and meltwater supply were terminated abruptly when the ice margin stepped back, first from the Salpausselkä I and later from the Salpausselkä II moraine. Isostatic rebound and the opening of seaways connecting the Baltic ice lake to the global ocean were responsible for drainage of the lake and the emergence of southern Finland (Bjorck &

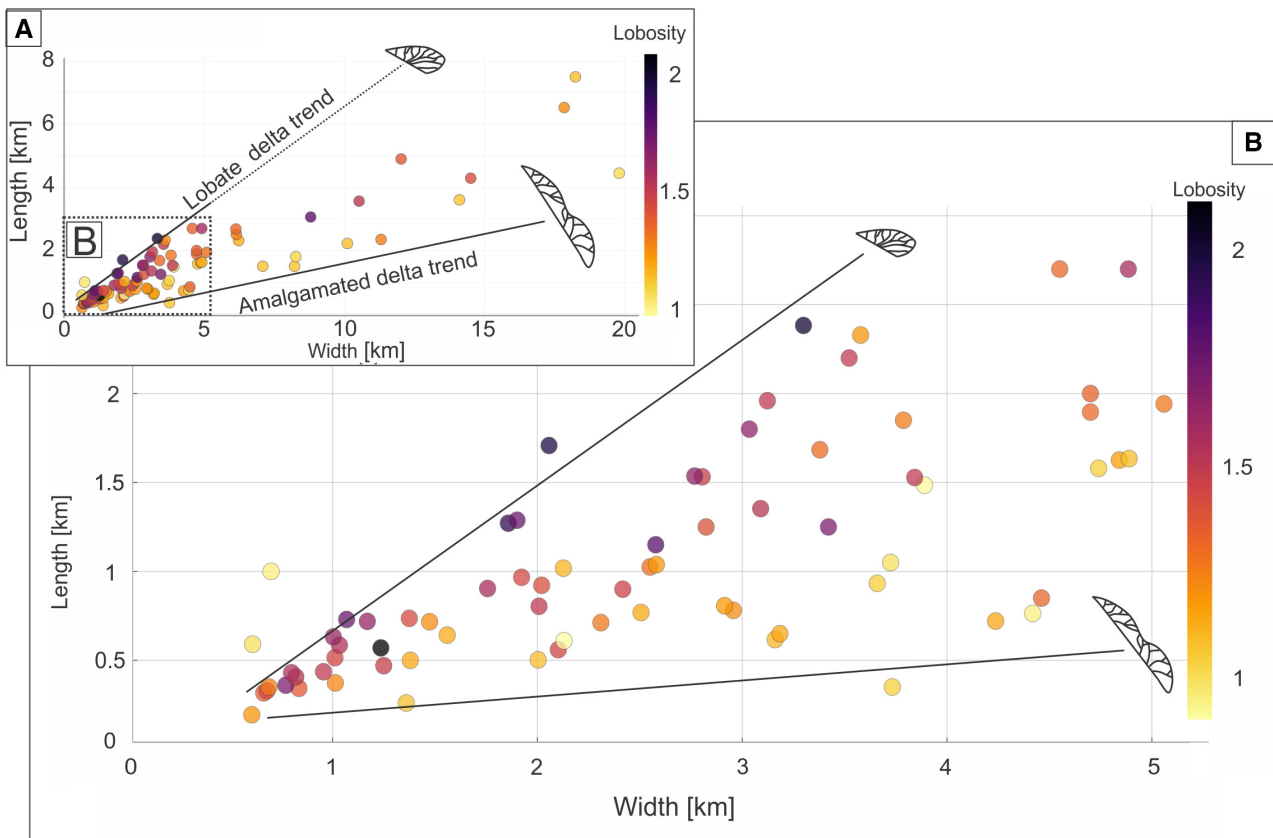


Fig. 4. Distribution of ice-contact delta metrics Salpausselkä I and II end moraines. Note that high lobosity is attributed to deltas <5 km in width and <3 km in length. Larger deltas tend to be an amalgamation of several individual lobate deltas. $N = 86$. (A) Distribution of metrics for all 86 deltas; (B) close-up on metrics of deltas below 3 km long and 5 km wide.

Digerfeldt, 1984; Glückert, 1995; Stroeven *et al.*, 2016). As a result, the deltas constitute high points in the present-day topography (Fig. 2).

Eskers

Sinuous or curvilinear, often discontinuous sediment ridges with steep sides (Fig. 2) running parallel or sub-parallel to the Younger Dryas Stadal ice-flow direction are observed (Fig. 1) (Johansson *et al.*, 2011). They are 8 to 40 m high (median 14 m), 16 to 920 m wide (median 78 m). The length of continuous segments ranges between 21 m and 17 400 m (median 174 m). The ridges often climb uphill and do not follow the topography. In places, ridges are flat-topped with numerous circular or irregular depressions. Smaller ridges are often amalgamating and anabranching, exhibiting a radial pattern and merge directly with the Salpausselkä ice-marginal ridges (Fig. 2).

The ridges are interpreted as eskers formed subglacially in meltwater conduits (Benn & Evans, 2010; Storrar *et al.*, 2014; Schomacker & Benediktsson, 2017). Meltwater flowed from north to south, driven by the ice-sheet surface slope (Shackleton *et al.*, 2018). Higher and longer eskers represent major meltwater paths draining farther into the interior of the ice sheet, whereas smaller ridges are interpreted as tributary meltwater channels located proximal to the ice margin (Fig. 2) (e.g. Storrar *et al.*, 2019). Their spatial relationship with ice-contact-deltas implies that the eskers acted as feeders, supplying sediment-rich meltwater to the ice margin.

Ice-contact delta metrics

Eighty-six deltas were identified along Salpausselkä I and Salpausselkä II. Their length, width and outer circumference were measured and a lobosity parameter was calculated following the

methodology outlined by Howell *et al.* (2008) (Fig. 4). The vast majority of deltas (82%) are <5 km wide and <3 km long (Fig. 4). Lobosity varies between 2.2 and 1.09 with the majority of deltas being <1.5 (Fig. 4). Low lobosity values are linked to amalgamated deltas in a 'bajada-style', where multiple point sourced fans grow to the lake surface forming point sourced deltas, which then coalesce to form one, bench-like delta, for example at Syrjälänkangas and Hyrtiälänkangas (Figs 2 and 4) (Barrett *et al.*, 2020a). Higher-lobosity deltas (>1.7) are clearly point sourced (for example, Vehivesmaankangas – Fig. 2). Two trends can be delineated from the distribution of dimension and lobosity data: (i) amalgamated deltas (length \ll width, with low lobosity); and (ii) lobate deltas (length \leq width, with high lobosity) (Fig. 4). Deltas with length \leq width but with low lobosity are constrained by topographic highs which prevent them growing laterally. The majority (88%) of deltas with lobosities >1.7 are <2.5 km long and <3.7 km wide (Fig. 4).

SEDIMENTOLOGY

Sixteen facies were identified, based on the dominant grain-size, sedimentary structures and the general expression in the outcrop (Table 1). Facies were then grouped into eight associations which have been distinguished from logs and outcrops based on the facies successions, dominant grain-size and sorting, sedimentary structures and position with respect to the ice margin at the time of deposition (Table 2). The latter is interpreted from the morphology of individual deltas (Fig. 2). The distribution of facies associations is described in the context of architectural elements comprising an ice-contact delta and juxtaposed against reflection patterns observed from GPR profiles (Figs 9, 10 and 11).

Architectural elements

Ice-contact slope

The ice-contact slope of the delta, where bulldozing and traction by ice are dominant, is characterized by boulder and cobble-sized clasts suspended in a fine-grained, silty and sandy matrix forming subglacial diamicton (FA1) (Table 2, Figs 5, 8H and 8I). Ice-margin advances/oscillations may cannibalize previously deposited, ice-contact fans forming high density

debris flows that descended the distal slope. As a result, the ice-contact slope is comprised of subglacial facies association (FA 1) mixed with ice-contact facies association (FA 2) (Figs 9 and 12).

The GPR profiles show that this mid to high amplitude, contorted or subparallel, discontinuous reflection package is present only on the ice-contact slope and in the top 1 to 6 m of the delta (Figs 10 and 11). Frequent hyperbolic reflections indicate large boulders incorporated within the matrix (Fig. 10A). Reflections typically dip in the opposite direction to the delta progradation direction. The depositional limit of this facies in the GPR can be correlated with push moraines visible in the delta morphology linking them to ice overriding (Figs 2 and 12).

Subaqueous ice-contact fan

Highly variable grain size and bedding dips are characteristic of subaqueous ice-contact fans (Table 2, Figs 5 and 9). Steeply dipping boulder and cobble gravels (FA 2) either pass sharply into, or are interbedded with, planar and low angle sinusoidally stratified and/or trough cross-bedded sands and gravels of FA 3 interpreted as cyclic step deposits (Fig. 8A and D) (Ghienne *et al.*, 2021; Lang *et al.*, 2021). FA 3 passes laterally into planar, ripple and climbing ripple laminated sands with the subordinate silty draping interbeds of FA 5 indicating initial high energy, supercritical flow (jet) deceleration, deposition of coarse fraction at the mouth of the meltwater portal due to flow expansion (FA 2) and transition from supercritical flow (FA 3) to subcritical flow (FA 5) (Figs 8A, 8B, 8C and 12) (Hornung *et al.*, 2007; Winsemann *et al.*, 2009). The facies transition is observed to happen on relatively short distances (tens of metres) laterally, as opposed to hundreds of metres in the down-flow direction (based on GPR data) possibly indicating a very high energy jet and highly supercritical flow conditions (Figs 8A and 12) (Hoyal *et al.*, 2003; Russell & Arnott, 2003; Hornung *et al.*, 2007; Winsemann *et al.*, 2009).

In GPR profiles the subaqueous ice-contact fan is characterized by low to high-amplitude, moderately dipping, semi-continuous reflections (Fig. 10A and E). Large contrasts in reflection amplitudes are most likely due to large variations in grain size and reflect variable energy of deposition between periods of high discharge (cobbles and boulders) and low discharge/flow

Table 2. Facies associations (FA) identified from sedimentary logs. Facies included in each association are listed in order, from the most to the least frequently described. The facies listed in brackets are less frequent or may not be present at all localities. For facies codes explanation see Table 1.

Facies association	Facies	Description	Interpretation
FA 1 Subglacial facies association	Dm	Boulder and cobble-sized clasts suspended in a silty and sandy matrix are typical of this facies association (Figs 5, 7I, 8E, 8H and 8I). Locally lenses or interbeds (<1 m thick, 2 to 10 m wide) of better sorted sands and gravels are observed within the succession. Some of them have distinct sharp edges and deformed primary bedding/lamination. Large turbate structures can be observed around boulders. This facies association has variable thickness (0 to 5 m), erosional basal surface and highly variable thickness distribution even at outcrop scale (10s m)	FA 1 is interpreted as traction till deposited subglacially (Evans <i>et al.</i> , 2006). When present on top of the succession, it represents a partial overriding of the delta by the ice sheet. Better sorted lenses/interbeds were either re-deposited as subglacially rafted freeze-on/rip-up clasts or deposited by subglacial meltwater at the ice-bed interface (Kessler <i>et al.</i> , 2012). Sandy and pebbly matrix together with partially preserved primary sedimentary structures (rippled lamination, low angle lamination) in some deformed beds indicates cannibalization and remobilization of fan/delta sediments
FA 2 Ice-contact facies association	Cmb, Cx, Gx, Gm, (Sp)	This facies association is found in the imminent vicinity of the ice margin. Steeply dipping (5 to 25°), planar, large-scale cross-bedded and massive, boulder-cobble gravels (0.2 to 0.8 m thick) with clasts up to 40 cm in diameter (most <20 cm) (Figs 5, 8A and 8D). In some beds a fining-upward trend is observed with occasional coarser/armoured top bed surfaces. Sand is either absent or very subordinate and/or confined to lenses in the leeside of larger boulders. Pebble gravel beds exhibit gentle fining-upward trend with more pronounced imbrication towards the top of the bed. This facies association shows sharp lateral contact with facies association FA3	FA 2 is interpreted to represent direct, ice-contact, fan sediments deposited almost immediately at the terminus of a subglacial conduit from high energy flows (Powell, 1990; Lønne, 1995). Massive or normally graded, planar cobble and boulder gravels may represent local hydraulic jump deposits with base scours larger than the width of the outcrop (ca 20 m) (Russell & Arnott, 2003; Winsemann <i>et al.</i> , 2009; Lang <i>et al.</i> , 2021). Some of the massive, poorly sorted cobble-boulder gravel beds may represent debris-flow deposits caused by discrete slope failures as the sediment pile passes the slope of repose or is bulldozed by the advancing ice margin. (Hornung <i>et al.</i> , 2007). Coarsening-upward packages with armoured top surfaces were formed as a result of winnowing by high energy jets which removed gravel and pebble fractions (Gobo <i>et al.</i> , 2014). Lower energy meltwater pulses deposited medium and coarse gravels with fining-upward trend due to waning flow energy. Cross-bedded gravels are interpreted as 2D/3D dunes (Russell & Arnott, 2003). Sand lenses were deposited in the flow shadow behind larger boulders indicating that most sand was winnowed or bypassed this zone. Sharp lateral contact of this facies association with FA 3 is interpreted as deposition in a large-scale (>20 m wide, >10 m high) axial scour of a jet efflux

Table 2. (continued)

Facies association	Facies	Description	Interpretation
FA 3 High energy fan/delta slope facies association	Gx, Gh, Gm, Cmb, Sp, Stx, Spx, (Sr, SFd)	Planar or low angle cross-bedded cobble-pebble gravels and sandy gravels (facies Cmb, Gx, Gh) as well as planar, low angle and trough cross-bedded sands and pebbly sands with strongly erosional bases are dominant in this succession (Figs 7F and 8A). They often form discontinuous lenticular bodies (2 to 10 m wide, 0.2 to 0.5 m thick) (depositional strike section). Planar laminated sand and pebbly sands 0.1 to 0.4 m thick are also present (Fig. 7H). The succession is often cross-cut by small-scale reverse faults. Gravel beds significantly incise and truncate finer grained strata. The dip of the strata ranges between 2° and 25°. Locally, convex lenses of massive cobble to pebble gravels (Cmb, Gm) with subordinate boulders are incised into underlying strata and overlapped by parallel laminated sands and sandy gravels above (Fig. 8A and C). FA 3 was observed to transition laterally into FA 5 over the distance of tens of metres (30 m in one of the outcrops) (Fig. 8A and B)	FA 3 is interpreted to be deposited subaqueously from fast-flowing glacial meltwater in a proximal subaqueous fan or steep delta slope setting (Lang et al., 2021). Multiple erosional contacts within low angle trough cross-bedded gravels are interpreted as progradation scour fills or chute-and pool deposits (e.g. Lang et al., 2017, 2021; Winsemann et al., 2018). Planar and low angle cross-bedded sands and pebbly sands were most likely deposited by breaking and non-breaking antidunes with wavelengths >10 m (Lang et al., 2021). Horizontal sands and pebbly sands are interpreted as upper-stage plane bed deposits deposited by bottom-hugging subcritical flows. It is noteworthy that the large wavelength of some of the bedforms makes it difficult to confidently identify bedforms in outcrop and distinguish between subcritical and supercritical conditions (Lang et al., 2021). Localized lenses of massive or crudely bedded boulder and cobble gravels are interpreted as debris-flow deposits (Fig. 8C and D). They include clasts of unconsolidated sand with preserved primary sedimentary structures (ripple marks, cross-bedding, etc.) (Fig. 8C), which are interpreted as frozen rip-up or bank collapse clasts and provide evidence for freezing conditions in the ice-marginal zone during deposition
FA 4 Delta foresets facies association	Stl, Spx, Gm, Gh, Sp, Stx, Sr, (Cmb)	Steeply dipping (10 to 35°), well-sorted, large-scale tangential (Stl) or planar (Spx) cross-bedding (2 to 10 m thick) (Figs 5, 6C, 6E and 8F) and smaller scale (0.2 to 1.0 m) planar (Spx) and trough (Stx) cross-bedding are prevalent through the succession (Figs 5 and 6C). Isolated lenses (1 to 5 m wide, 0.5 to 2.0 m deep) of massive and/or planar cross-bedded gravels. This facies association appears remarkably uniform in outcrop with the majority of grain sizes within the coarse and medium sand fractions (field measurements) (Figs 6C, 6E and 8F). Erosional scours (0.5 to 2.0 m wide, <1 m deep) and filled with a gravel lag followed by a trough cross-bedded sand package are also observed in outcrop. The top part of the steeply dipping FA 4 is	FA 4 is interpreted as Gilbert-type delta foresets deposited from expanding flows of sediment-laden meltwaters. Variation in depositional dip direction on outcrop scale suggests lobe switching and/or deposition from multiple sediment input sources (braided channels). Large-scale planar cross-bedded sands (Spx) are interpreted as a product of hyperpycnal or homopycnal flows travelling down the steep delta slope (Fig. 8F) (Gobo et al., 2014, 2015). Large-scale tangential cross-beds (Stl) are interpreted as aggrading backsets of cyclic steps deposited from supercritical flows filling long-wavelength erosional scours (Winsemann et al., 2009; Dietrich et al., 2016; Lang et al., 2021). Trough cross-bedded sands (Stx) represent 3D dunes and

Table 2. (continued)

Facies association	Facies	Description	Interpretation
FA 5	Sp, Spx, Sr, Scr, SFd, Fd, SFc, (Stx Spx Gm, Gh)	truncated by facies association FA 6 exhibiting sharp, erosional contact (Fig. 8F). The depositional dip azimuth measured from outcrops ranges between 134 to 272°. Variation of both dip angle and dip direction occurs even at the outcrop scale (tens of metres)	antidunes deposited from transitional (supercritical–subcritical) flows (Alexander <i>et al.</i> , 2001; Dietrich <i>et al.</i> , 2016; Winsemann <i>et al.</i> , 2018). Sand and gravel-filled scours represent chute-and-pool deposits (Lang <i>et al.</i> , 2021). Lenses of clast-supported, massive or crudely bedded conglomerates (Cmb) are interpreted as debris flows associated with high magnitude events transporting the coarse fraction from delta topsets down the delta front (Lin & Bhattacharya, 2020). They are present mainly towards the bottom of the foresets, possibly indicating a foreset-toeset transition and turbid meltwater plume deceleration due to the decrease of the delta slope. Some of the coarse fractions were likely supplied to the slope break and avalanched along the delta, ultimately forming debris-fall lenses in the toe of the foreset slope (Gobo <i>et al.</i> , 2014)
FA 5	Sp, Spx, Sr, Scr, SFd, Fd, SFc, (Stx Spx Gm, Gh)	Medium, fine and very fine sands are dominant in this facies association. The most typical succession consists of planar bedded sands/pebbly sands followed by ripple and climbing ripple laminated sands and locally capped with horizontal or draping laminated fine and very fine sands/silts (Fig. 8B) (Sp → Sr (Scr) → SFd/ Fd). Individual beds are dipping between <1° and 10° and vary in thickness between 5 to 70 cm. Subordinate, coarser packages of low angle planar and trough cross-bedded sands and pebbly sands are locally present. Contorted sands and silts with very prominent soft sediment deformation structures (SSD): load clasts, ball-and-pillows and complex folds are common (Fig. 6A and B). In the most distal part of the delta, soft sediment deformation exhibits a characteristic facies succession: medium, well-sorted cross-bedded sands, overlain by contorted sands and silts and capped by draping and planar laminated silts and sands (Fig. 5)	This facies association is interpreted as low-energy fan/delta bottomsets. The fining-upward succession represents waning meltwater pulses transitioning from upper plane through current type A and type B climbing ripples and draping lamination deposited after the flow decelerated below ripple migration threshold (Ashley <i>et al.</i> , 1982). The contorted sands with soft sediment deformation structures (SSD) (Fig. 6A and B) are interpreted as slump deposits. From outcrops, it appears that shearing and sliding along a slip surface, possibly gravity driven, occurred within the cross-bedded sandy package. As a result, more cohesive silts and fine sands are contorted and folded together with a portion of the underlying coarser sand package, which acted as a 'ball bearing' sub-stratum rather than a clear, planar detachment surface. Following slumping, wavy and planar laminated fine sands and silts were deposited from suspension, capping the sequence. Similar SSDs have often been attributed to earthquakes, resulting from glacial isostatic rebound (Gruszka & van Loon, 2007; Loon & Pisarska-Jamrozny, 2014; van Loon

Table 2. (continued)

Facies association	Facies	Description	Interpretation
FA 6 Delta topsets facies association	Gm, Gx, Gh, Sh, Cmb, Cx, Ch, Stx, Spx	FA 6 is found in the uppermost part of the succession (1 to 6 m). It is composed of massive, planar and cross-stratified cobble and pebble gravels with subordinate sands (Figs 5 and 8G). (Cmb, Cpx, Ch, Gm, Gx, Gh). The sediments are either flat-lying or dipping very gently (ca 1°) following the general dip of the plateau surface. Multiple, erosional base and top facies contacts are observed (Figs 7D and 8G). Particle diameter is highly variable but rarely decreases below pebble gravels. Individual clasts can reach up to 1 m in diameter in the ice-proximal part of the delta (Fig. 7D). Pebble to boulder imbricated gravel packages can be traced both in the depositional strike and dip directions on the scale of metres to tens of metres (typically <30 m). Lenticular or U-shaped bodies (length 1 to 8 m, height 0.4 to 1.2 m) with erosional base and filled with massive or crudely bedded sediments which are coarser than neighbouring facies are locally present (Fig. 8G). The coarse sediments are interbedded with subordinate coarse and medium sands (Sp, Spx, Stx) which are either filling voids between larger clasts or form a 'tail' on the lee side of larger boulders or cross-bedded gravel sets	<i>et al.</i> , 2016). However, slumping in the study area is more likely to be related to autogenic processes of delta progradation, when the slope of the delta exceeds the slope of repose (Pisarska-Jamroz & Weckwerth, 2013), which may be exacerbated by fluctuating lake-water levels. The finer grain sizes are often characteristic of delta bottomset/prodelta environments (Mastalerz, 1990; Postma, 1990; Nemeč & Postma, 1993). However, FA 5 has been also described from a site very close to the ice margin <i>ca</i> 60 m laterally from the mouth of an interpreted meltwater portal (Fig. 8A and B)
FA 7 Large distributary	Cmb, Ch, Gm, Gh, Gx	The succession has been interpreted to represent a braided delta top, which is reinforced by the morphology of the plateau, with remnants of channel networks still clearly visible (Fig. 2) (e.g. Glückert, 1986; Fyfe, 1990; Postma, 1990; Winsemann <i>et al.</i> , 2018). As a result of little or no accommodation and high energy of glaciofluvial depositional environment, multiple erosional internal contacts between facies are present. Lenticular concave up bodies of coarse pebble and cobble gravels are present and interpreted as channel-fill deposits. Some isolated pockets of cobble and boulder gravels may also represent supercritical flow deposits associated with local hydraulic jumps formed at obstacles or backsets of antidunes (Russell & Arnott, 2003; Lang <i>et al.</i> , 2021). Planar cross-bedded pebble and cobble gravels are interpreted as mid-channel bars, migrating downstream. Bedforms associated with subcritical and supercritical flows are present within the succession indicating variable flow regimes in line with seasonality of glacial meltwater discharge (Marren, 2005). Preservation of sands mainly in flow shadow zones indicate that the meltwater energy was high enough to either erode or prevent sand from depositing, and that most of the sand bypassed delta topsets	FA 7 is interpreted as a channel fill formed during a major meltwater drainage event which incised the delta

Table 2. (continued)

Facies association	Facies	Description	Interpretation
channel facies association		(Gm, Gh) and with clear erosional base incising into delta topsets (FA 6) and delta foresets (FA 4) down to 6 m can be observed in the outcrop (sediment log 4 – Figs 5A and 6E). It can be traced laterally for over 200 m to where it pinches out. The maximum and the average grain size of the clasts is visibly bigger than in FA 6 (average 25 cm, maximum ca 80 cm – Fig. 6F). Boulder and cobble gravel beds are discontinuous with erosional internal contacts (Fig. 6E). The location of the outcrop (sediment log 4 – Fig. 5A) corresponds to a large distributary channel observed in the DEM (Fig. 2 – location 4). The channel is cross-cutting some of the distributary channel network on the delta top implying that it was active after the topsets were deposited (Fig. 2). Three similar channels are observed from delta morphology in the study area. They are 900 to 1800 m long, 50 to 250 m wide and incise delta tops between 3 m and 11 m (Fig. 2 – Hyrtiälänkangas and Kukunkangas)	topsets either as a response to the Baltic ice lake base level drop or as a consequence of an outburst flood (Brookfield & Martini, 1999; Gomez <i>et al.</i> , 2000; Winsemann <i>et al.</i> , 2009, 2018; Gobo <i>et al.</i> , 2015; Lang <i>et al.</i> , 2021). The channel most likely developed following ice-marginal retreat from Salpausselkä I when an ice-contact lake that developed between the ice sheet and the proximal delta slope of Salpausselkä I overspilled and drained southward into the Baltic ice lake (Fig. 2). High energy of the flow is reflected in sediment grain size within FA 7 which ranges from cobble to boulder-sized gravels and massive or poorly bedded structure of the deposits pointing towards a high-magnitude event
FA 8 Kettle hole facies association	SFd Fwh, Scr SFc, Sr, Sp, (Gm)	Fine, planar or draping laminated sands and silts characterize this facies association (FA 7) (Figs 5, 7A, 7B and 7C). Interbeds of coarser, ripple (Sr) and climbing ripple-laminated (Scr) sands, and isolated lenses of massive gravels (Gm), together with contorted sands (SFc), are also present (Fig. 5 – log 6; Fig. 7B and C). An outsized clast of +60 cm in diameter is clearly visible in the centre of the section (Fig. 6C). It appears to be disturbing the layers in its vicinity, but evidence for impact structures is absent (e.g. Domack & Lawson, 1985; Bennett <i>et al.</i> , 1996). The succession itself is well-exposed in the outcrop (Fig. 7A). In the outcrop this facies association can be observed to form isolated, irregular and laterally thinning fine sediment bodies, onlapping onto the host succession (FA 6, FA 2). Small-scale normal faulting can be observed	FA 8 is interpreted to be a kettle-hole lake fill succession that developed during and after a buried ice block was blanketed by delta topset sediments and, subsequently, melted out (e.g. Maizels, 1977; Wingfield, 1990; Benn & Evans, 2010; Götz <i>et al.</i> , 2018). Melting of the ice block created localized accommodation, probably a small lake, which was infilled with fine-grained sediment. The outsized clast is interpreted as a 'slide-stone', which travelled down along the slope as the walls of the kettle hole (Fig. 7C). Ice melting, leading to the loss of lateral support, is deemed responsible for the presence of small-scale normal faults (Fig. 7B). Similar normal faults are reported to form due to the reactivation of basement faults but given the morphological context it is unlikely in this case (e.g. Brandes <i>et al.</i> , 2011). This association is remarkably similar to the low energy fan/delta bottomsets association (FA 5) making it difficult to interpret it without the context of neighbouring sediments (FA 6) (Fig. 7A) and the geomorphology revealed by the high-resolution DEM

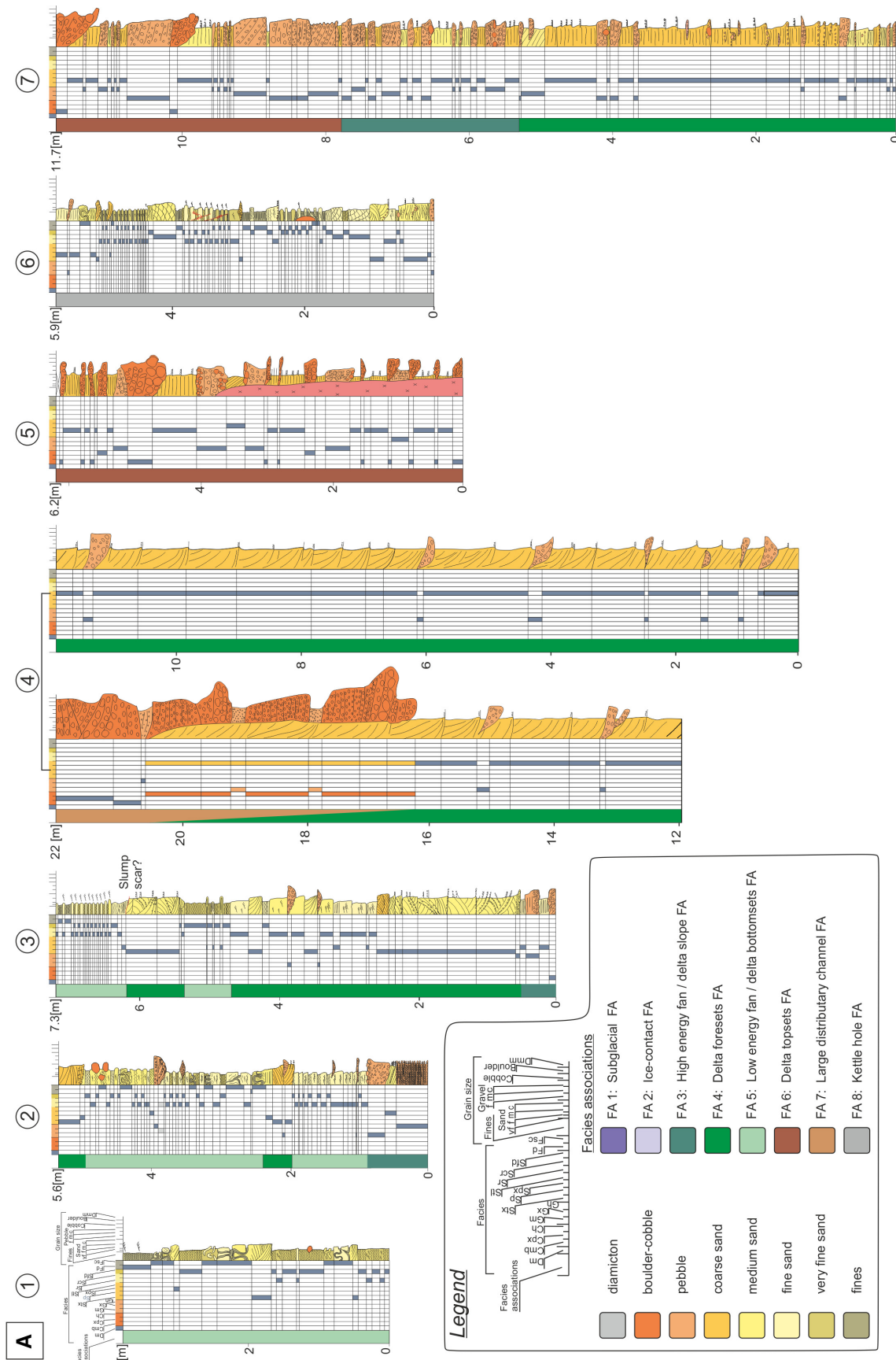


Fig. 5. Sedimentary logs: (A) logs 1 to 7; and (B) logs 8 to 14. For location see Fig. 2. Grey areas designate identified facies which were used to distinguish facies associations (FA 1 to FA 8 on the legend).

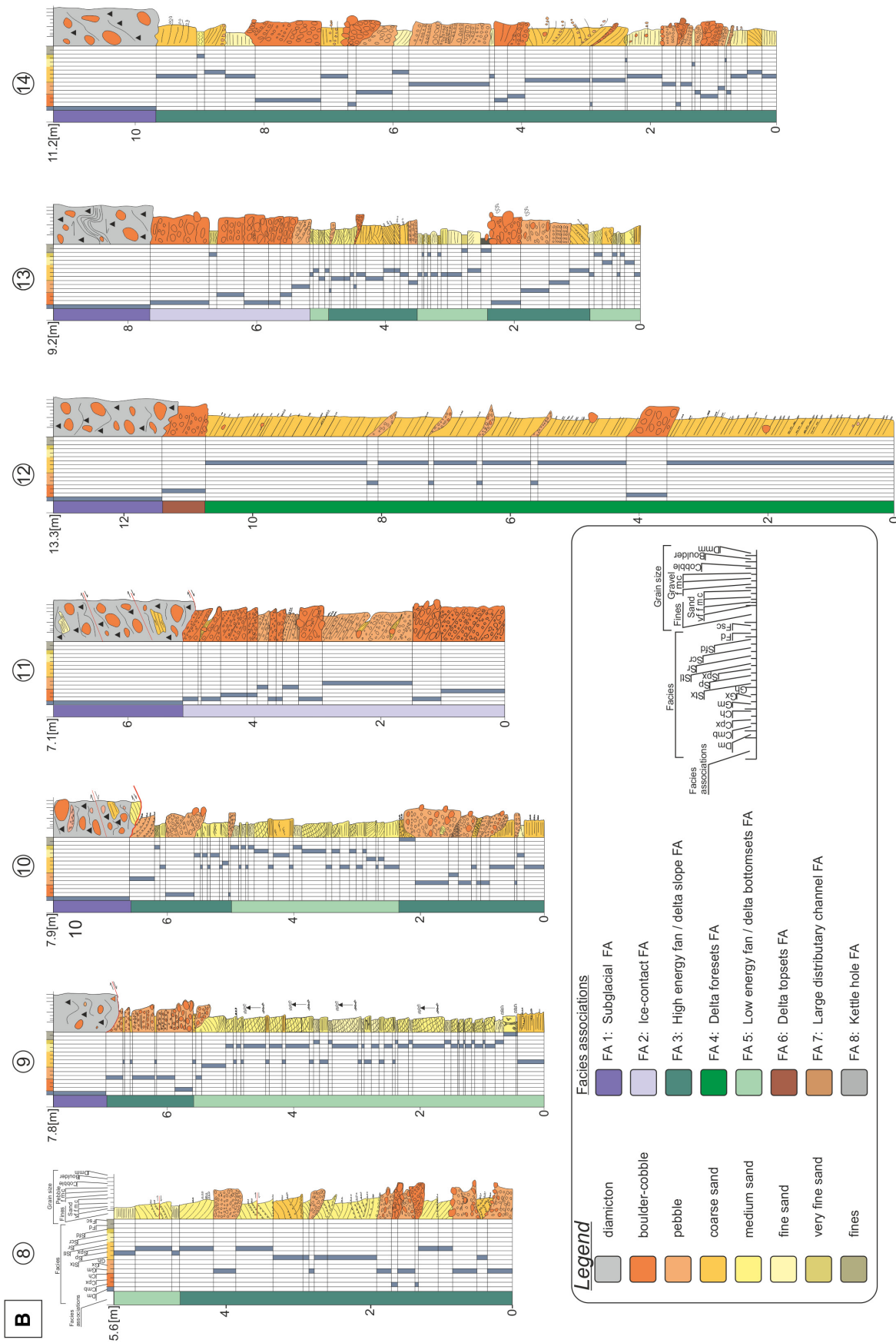


Fig. 5. Continued

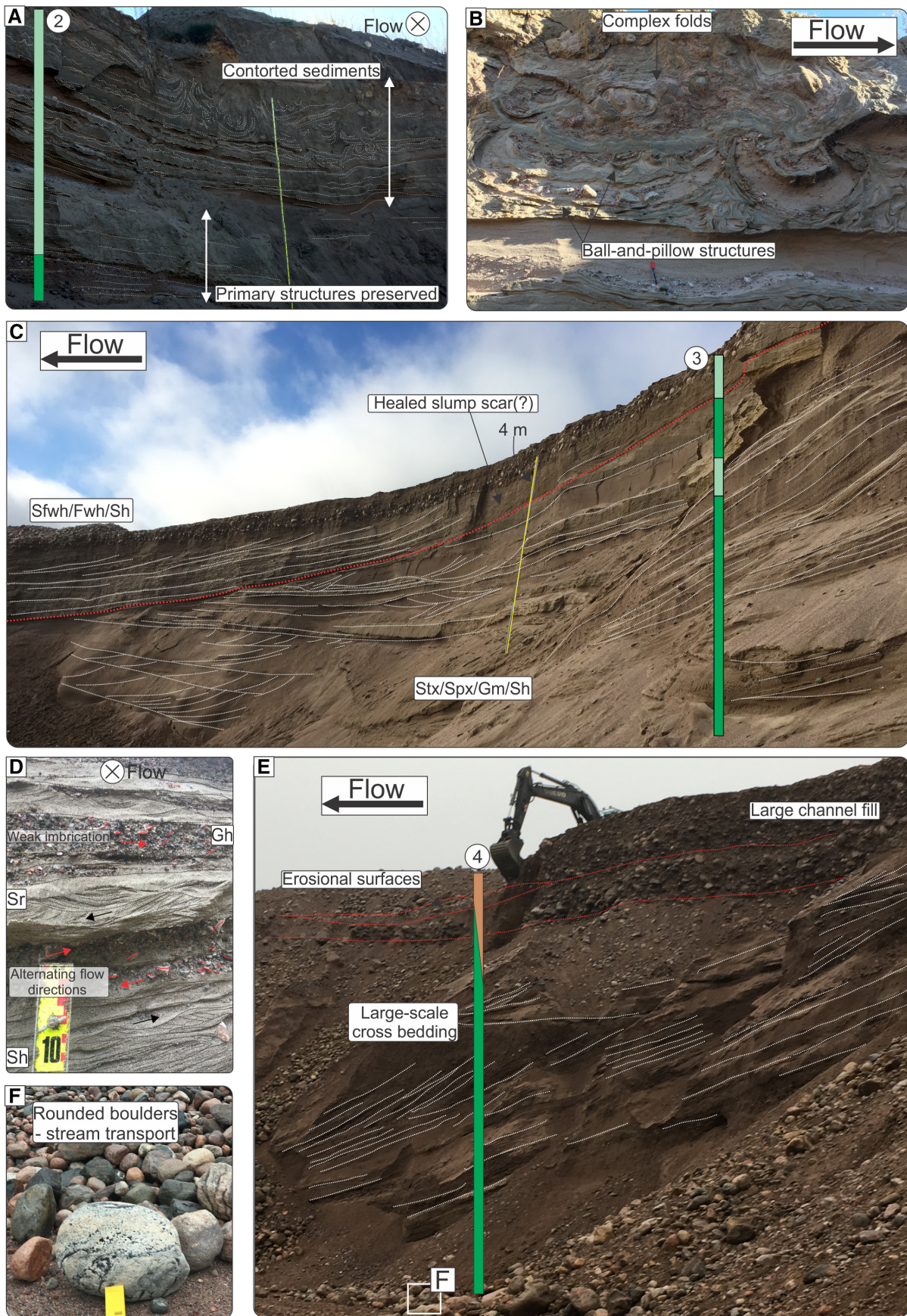


Fig. 6. Details of sediments found in outcrops. Log locations indicated by coloured bars and corresponding circled number. (A) and (B) Contorted and fine sediments in the distal delta bottomsets; (C) discordant contact between sands (bottom) and finer sediments above the suspected slump scar in delta foresets, note cut-and-fill structures as well as cross-bedding in the direction opposite to the delta slope possibly indicating backsets cyclic steps and/or upslope-migrating antidunes; (D) interbedded sands with current ripples preserved and gravels with weak imbrication. Note alternating current direction indicators which may point to deposition from 3D dunes or cyclic steps; (E) outcrop of the medial (along the depositional dip) part of the delta. Note large-scale cross-bedding unconformably overlain by massive and crudely stratified cobbles and pebble gravels of a large distributary channel; (F) size of some boulders transported within the channel was in excess of 80 cm in diameter.

cessation (fine sands and silts) (Fig. 5B, log 13, and Fig. 12) (Marren, 2005).

Delta foreset

Wedge-shaped, steeply dipping well-sorted, coarse sands and pebble gravels of FA 4 constitute the majority of the delta foresets (Table 2, Figs 5, 6C, 6E and 8F). Steepness of the delta foresets (up to 35°) favours deposition from supercritical density flows either in the form of antidunes or cyclic step deposits (Fig. 8F) (Winsemann *et al.*, 2018; Ghienne *et al.*, 2021; Lang *et al.*, 2021). Subordinate coarser deposits of FA 3, in the form of lenses, represent either high density debris flows due to high magnitude meltwater events remobilizing topset facies (FA 6 and FA 7), larger hydraulic jumps or debris-fall lenses originated from failures of the upper delta slope (Fig. 5) (Russell & Arnott, 2003; Nemeč *et al.*, 2008; Lang *et al.*, 2017a; Winsemann *et al.*, 2018). Subcritical flow deposits formed during periods of low meltwater discharge or in areas where flows decelerated, and are characterized by planar and trough cross-bedded, and rippled sand of FA 5 (Figs 5 and 6C).

In GPR profiles delta foresets are characterized by large, steeply dipping reflections with variable amplitudes (Figs 10 and 11). Some reflections are continuous throughout, and show clear offlap from, delta topsets whereas others are either truncated or show a toplap relationship (Fig. 10A and C). Variations in reflector architecture are attributed to the changing base level of the Baltic ice lake (Backert *et al.*, 2010; Winsemann *et al.*, 2011, 2018). Low reflectivity zones within the delta foresets are interpreted as uniform sediment composition (i.e. grain size) generated under stable discharge conditions (Fig. 10A and B). Higher reflectivity represents an increase in electrical permittivity contrast, probably resulting from variations in grain size due to flow cessation (lobe switching) and deposition of finer grained sediment drapes from suspension or, discharge increase and deposition of

coarser lithologies (boulders or cobbles). In GPR profiles perpendicular to the depositional dip, delta foresets appear as semi-continuous, sub-parallel, sinusoidal reflectors (Figs 10C and 11) prograding at up to *ca* 90° from the main depositional dip direction (i.e. towards the west or east) (Figs 10C and 11). Variations in the progradation direction often occurred in the vicinity of pronounced bedrock highs, where meltwater flow was locally deflected. Foreset reflections pass distally into more shallow dipping and higher amplitude packages interpreted as delta bottomsets (*cf.* *Delta bottomsets* section).

Delta bottomsets

Delta bottomsets are characterized by shallower dips and finer grain size than the delta foresets (Figs 5, 6A, 6C, 9 and 12). Deceleration of bottom-hugging meltwater plumes due to the shallower angle of dip and dilution of the flows resulted in deposition in subcritical conditions (Froude number <1) (Gobo *et al.*, 2014; Kostic *et al.*, 2019). FA 5 is characterized by repeated, fining-upward succession of sands with upper plane bed, ripple and climbing ripple lamination into sands and silts that were deposited from suspension suggesting gradual waning energy of the flow (Table 2, Figs 5 and 8B). Coarser packages of sand and pebbly sand (FA 4) are also present but constitute a minor component (Table 2, Figs 9 and 12). Outsized lenses of massive/coarser cobble gravels (FA 3) are interpreted as debris-fall lenses (*cf.* *Delta foreset* section) deposited in the toe zone of the foreset/upper part of bottomset (Table 2, Fig. 12) (Barrett *et al.*, 2020a).

In GPR profiles delta bottomsets are identified as downdip continuations of foresets exhibiting a clear change to a shallower dip angle and increase in amplitude (Fig. 10). Reflections are semi-continuous and often onlap onto bedrock topographic highs (Figs 10A, 10C, 10D and 11). Delta bottomsets may pass into, or be



Fig. 7. (A) Contact between kettle hole sediments (log 6) and topset facies (log 5). Note the exposed bedrock high. (B) and (C) Details of kettle hole sediments. Small-scale normal faults likely due to loss of support by melting of a buried ice block. Shovel for scale is 1.2 m long. (D) Detail of proximal/topset facies. (E) Striae on bedrock surface indicate local ice flow direction towards the south-east. (F) Section by log 8. (G) Small scour-and-fill structure. Similar lenses were abundant within the section. (H) Small-scale folding and thrusting caused by ice-margin oscillation. (I) Detail of a thrust plane filled with very fine silt/clay implying that water was injected into the thrust plane. Pencil for scale is 15 cm long.

interbedded with, prodelta deposits (cf. *Prodelta/lake bottom sediment* section). They are observed in GPR data as higher amplitude, more continuous reflections attributed to higher water content in the fine-grained sediments (Fig. 10A and D). The thickness of delta bottomsets is controlled by the underlying bedrock topography and can be extremely variable from 0 m in areas where bedrock crops out to over 60 m in troughs, as confirmed by boreholes (Figs 11 and 12).

Delta topsets

Delta topsets can be observed in the uppermost part of some outcrops (1 to 6 m) as a coarse, bedded package of pebble and cobble gravels with subordinate cobble gravels and sands which truncate the foresets (Figs 5, 7A, 7F, 8F, 9 and 12). The topsets were deposited subaerially by braided glaciofluvial meltwater streams originating at the ice margin (e.g. Fyfe, 1990; Postma, 1990a,b; Thomas & Chiverrell, 2006; Rohais *et al.*, 2008). Limited accommodation and periodic high discharges led to the erosional character of FA 6 (Table 2, Fig. 9). Cobble and boulder gravels were transported mainly as bedload whereas most of the sands and finer fraction bypassed the delta topsets or was deposited during the waning flow stage, and then winnowed by subsequent higher meltwater discharges (Burke *et al.*, 2010; Pisarska-Jamroz & Zieliński, 2014). Base level fluctuations of the Baltic ice lake led to incision and reworking of some of the topsets (FA 6) and foresets (FA 4) when the lake level fell, versus aggradation of topset sediments, when the lake level rose (Fig. 12) (Winsemann *et al.*, 2011).

In GPR profiles topsets are characterized by a semi-continuous or continuous, high-amplitude, horizontal reflection package (Fig. 9). The package usually spans the whole length of the delta and terminates at the delta brink. Some topset reflections are observed to offlap and pass into delta foresets showing either a progradation or an aggradation and progradation stacking pattern when the delta brink was responding to rising

lake levels (Fig. 9A and D) (Brookfield & Martini, 1999; Gobo *et al.*, 2015; Winsemann *et al.*, 2018).

Large distributary channel

Several large distributary channels attributed to high magnitude meltwater discharge events are visible in the delta morphology (Figs 2, 10B and 12). In outcrop they are represented by a very coarse, laterally tapering package of crudely bedded boulders and cobbles with multiple reactivation surfaces (Figs 5, 6E and 6F).

Several such channels >50 m wide were observed in GPR profiles (Figs 9 and 10C; Appendix S1). They are characterized by concave, mid to high-amplitude basal reflections filled with semi-continuous reflections some of which onlap onto the basal reflector (Fig. 9). Secondary, smaller concave reflectors are present within the channel fill facies and can be correlated to internal erosional surfaces present in the outcrop (Fig. 9). One of the underfilled channels, visible in the delta morphology, can be linked to a semi-transparent foreset package interpreted as a product of a large meltwater drainage event (possibly a lake outburst flood) or an incision due to lake level fall (Fig. 10B). The semi-transparent reflection is interpreted as deposited from a sustained flow associated with high-magnitude drainage events resulting in the deposition of a uniform sedimentary package (Clague & Evans, 2000; Winsemann *et al.*, 2011; Westoby *et al.*, 2014).

Kettle holes

Oval or irregular kettle holes cover up to 20% of the delta surface (Fig. 2) (Girard *et al.*, 2015; Maries *et al.*, 2017). Such depressions are often fully or partially filled with fine sediments of FA 8 (Table 2, Figs 5, 9 and 12). The sediments are remarkably similar to the delta bottomsets (Fig. 9) and it would be extremely hard to identify a kettle hole fill without the context of neighbouring facies (FA 6 and FA 7) (Fig. 8A, B, C and D) and the geomorphology revealed by the high-resolution DEM (Fig. 2). If encountered in well or borehole, without the geomorphological context,

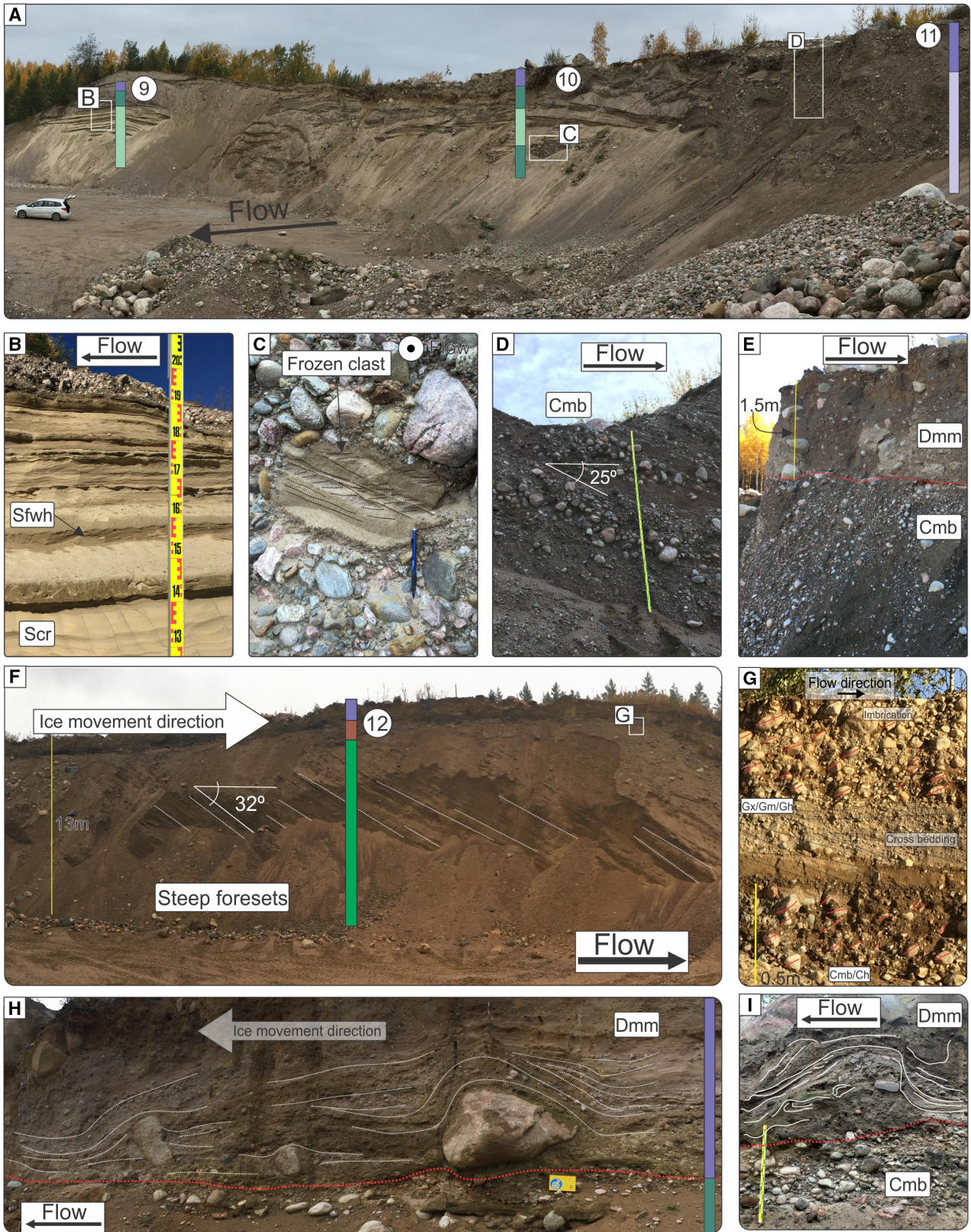


Fig. 8. (A) Outcrop where logs 9, 10 and 11 were taken. Logs are very different even though the distance between them is small. The section lies parallel to the palaeo-ice margin. (B) Alternating climbing ripple packages fining-upward to draping lamination, each indicating waning flow energy. (C) Sandy rip-up(?) clast with preserved primary bedding within a debrite deposit indicating that the clast was frozen during deposition. The clast is embedded in a massive cobbly conglomerate package. Pencil for scale is 15 cm long. (D) Alternating, steeply dipping massive cobbles and gravels. (E) Contact between massive subglacial diamicton and poorly sorted proximal facies. (F) Steeply dipping sandy foresets unconformably overlain by thin topset facies. The whole package is capped by subglacial diamicton implying ice overriding. (G) Detail of topset facies. (H) and (I) Detail of subglacial diamicton facies and contact with underlying ice-proximal packages.

the succession could be misinterpreted as more laterally extensive muds associated with flooding of the delta. (Figs 5 and 12).

In GPR data possible filled kettle holes are identified as high-amplitude convex packages with reflections ‘filling’ the initial depression (Figs 9 and 10C; Appendix S1). As per bottom-set sediments, the elevated amplitude response is linked to increased water retention within the fine-grained sediments.

Esker

Deposits associated with eskers have not been encountered in outcrop and are identified based on their morphological expression linked to the GPR profiles where they exhibit a broad range of responses from medium-amplitude semi-chaotic reflection patterns to almost transparent with some discontinuous, steeply dipping, reflections (Figs 9 and 10D; Appendix S1). Typically, sediments forming eskers range from boulders and cobbles (high discharge) to sands and pea gravels (low/waning discharge) (Fig. 12) (Burke *et al.*, 2015; Knight, 2019). An esker may have a complex geometry due to filling only a part of the subglacial conduit or fully filling a complex subglacial, englacial or supraglacial, or combination thereof, drainage network (Fig. 12C and D) (Artimo *et al.*, 2003; Mäkinen & Palmu, 2008; Gruszka *et al.*, 2012; Storrar *et al.*, 2019). Higher amplitude reflection packages delineating the top of the esker which are onlapped and or draped by subaqueous ice-contact fan/delta foresets are common diagnostic features (Fig. 12). The higher amplitude is attributed to deposition, from suspension, of overlying fine fractions on top of a submerged esker after the ice margin had retreated. It may not be possible to identify buried eskers/ice marginal sediments solely from the GPR profiles as they are difficult to reliably differentiate from bedrock highs and have similar dielectric permittivity values to neighbouring sediments (Fig. 11).

Prodelta/lake bottom sediment

Prodelta sediments were also only interpreted from GPR profiles (Figs 9 and 10A). They are a distal continuation of the deltaic bottomsets (Fig. 10A; Appendix S1) and are characterized by continuous, subparallel, high-amplitude reflections (Fig. 9). Baltic ice lake fine-grained sediments are known from other localities, to have high silt/clay content, which is consistent with their high reflectivity in the GPR data (Figs 10A and 11) (Donner, 2010; Hyttinen *et al.*, 2011; Zolitschka *et al.*, 2015). Thicker, high reflectivity packages occur in bedrock depressions and in areas down-flow from bedrock knolls (Fig. 10A and C). In GPR profile 16 (Fig. 11) a higher amplitude layer of silt/clay draping part of the delta is confirmed by wells. It is interpreted to represent deposition from suspension over an inactive, submerged, part of the delta during a period when meltwaters were diverted to the west, possibly due to an ice margin re-advance over the proximal part of the delta (Fig. 2).

Summary of sedimentary environments

From outcrop and GPR data it is apparent that facies distributions within the delta are more complex than typical Gilbert-type deltas. Rapid lateral and proximal–distal facies variations are linked to supercritical/subcritical flow transitions which are characteristic of ice marginal and subaqueous ice-contact fan/delta systems (e.g. Russell & Arnott, 2003; Hornung *et al.*, 2007; Winsemann *et al.*, 2009, 2018; Dietrich *et al.*, 2016; Ghienne *et al.*, 2021; Lang *et al.*, 2021). Correlation of logs, even at the outcrop scale, is challenging (Figs 5, 7F, 8A and 12). GPR data suggest that subaqueous ice-contact fan deposits extend 200 to 400 m (maximum 600 m) from the former ice margin (Figs 9A and 12; Appendix S1). This distance is a function of the energy of the meltwater jet, angle of repose of the ice-contact fan sediments and the water depth of the Baltic ice lake


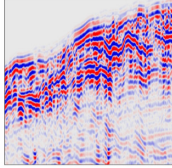

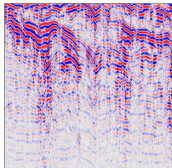

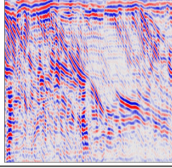

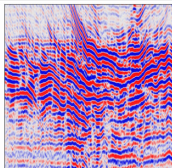

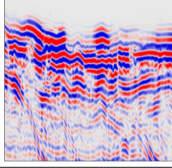

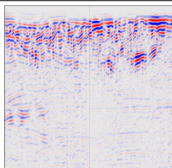

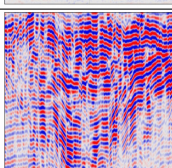
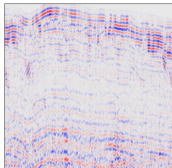
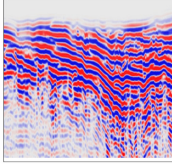
Architectural element	Facies associations (): subordinate (()): rare	Geometry <i>l</i> : length, <i>w</i> : width, <i>h</i> : thickness, α : angle of bedding	Synthetic log	GPR facies	Reservoir properties
Ice-contact slope	FA 1, (FA 2)	<i>l</i> : 10s m <i>w</i> : corresponding to the delta width <i>h</i> : 1 - 20 m α : -20° - < 1° dips in the opposite direction to delta progradation (ice-contact slope), sub horizontal when on delta surface			Poor
Subaqueous ice-contact fan	FA 2, FA 3, (FA 5) ((FA 1)),	<i>l</i> : 50 - 400 m (> 600 m) from the ice margin, <i>w</i> : 10s - 100s m, <i>h</i> : 10 - 60 m α : up to 25° in close to the ice margin decreasing distally to 2°			Good / moderate
Delta foresets	FA 4, (FA 3), (FA 5)	<i>l</i> : length of the delta reduced by length of the fan <i>w</i> : 100s - 1000s m <i>h</i> : 5 - 30+ m α : 10° - 30°			Very good
Delta bottomsets	FA 5, (FA 4), ((FA 3))	<i>l</i> : corresponding to the length of the delta, <i>h</i> : 5 - 25 m (max 60 m) α : 1° - 10°			Good / moderate
Delta topsets	FA 6, (FA 7)	<i>l</i> & <i>w</i> : corresponding to the dimensions of the delta <i>h</i> : 1 - 6 m, α : < 1°			Very good
Large channel	FA 7	<i>l</i> : 800 - 1900 m <i>w</i> : 50 - 300 m <i>h</i> : 3 - 12 m			Very good
Kettle hole	FA 8	<i>l</i> : 10s - 100s m <i>w</i> : 10s - 100s m <i>h</i> : 2 - 30 m (<i>l</i> , <i>w</i> & <i>h</i> highly variable- See Figure 2)			Good / moderate
Esker	Not present in outcrop	<i>l</i> : 100s - 1000s m <i>w</i> : 10s - 100s m <i>h</i> : < 50 m			Good
Prodelta / Lake varves	Not present in outcrop	n/a			Poor

Fig. 9. Architectural elements of ice-contact deltas identified from outcrops and juxtaposed against GPR reflection patterns observed from GPR profiles. Reservoir properties are described qualitatively based on visual inspection of outcrops, and field assessment of grain size, sorting and content of fine fractions. Where no outcrops were available, reservoir properties are assessed based on available literature: (Zolitschka *et al.*, 2015; Maries *et al.*, 2017).

(Hoyal *et al.*, 2003; Winsemann *et al.*, 2009; Gobo *et al.*, 2015; Lang *et al.*, 2017, 2021). In ice-contact settings delta and fan facies are genetically linked and exist on a spectrum, i.e. when a subaqueous fan reaches the lake surface or the lake level falls, deposition of a Gilbert-type delta commences. The delta then progrades into the basin until the sediment supply ceases or the lake level rises again above the delta topsets, in which case fan sedimentation takes over and may ultimately overtop the delta (Lønne, 1995; Thomas & Chiverrell, 2006). Deflection of delta foresets around bedrock highs and ponding/preferential settling of finer fractions (bottomsets and prodelta sediments) in bedrock lows can be identified from GPR profiles (Figs 10C and 11). In some cases, older, pre-existing sediments associated with previous ice-margin positions and/or eskers can be buried by delta progradation as observed in GPR data (Figs 9D and 12). Two alternatives, and equally likely, scenarios for the formation of a buried sediment body are considered here (Fig. 12C and D). Irrespective of their genesis, such sediments can be draped with prodelta muds during the time between ice-margin retreat and the progradation of the delta foresets over them (Figs 11 and 12). Subglacial diamicton (traction till) is usually present on the proximal slope and on the delta top, if ice advanced over it, but it may be patchy or absent, if the ice margin was less active (Fig. 12). Underfilled kettle holes are more abundant in the ice-proximal part of the delta (Figs 2 and 12). When kettle holes are filled, typically with fine-grained sediments, they introduce further heterogeneity to the deltaic package (for example, Figs 7A, 7B, 7C and 12). Given the scale of the system, the above detail is unlikely to be imaged in the subsurface by standard seismic exploration methods (e.g. Barrett *et al.*, 2020).

ELECTRICAL RESISTIVITY TOMOGRAPHY

The ERT profiles penetrate the sedimentary succession to depths between 30 m and 70 m (Fig. 13; Appendix S1). Four distinctive resistivity zones are identified (Fig. 14). The highest resistivity values

were recorded in the upper 10 to 20 m of zone 1 (Z1) with values between 12 000 to 120 000 Ωm (mean: 49 700 Ωm , four iterations). In profiles 1 and 3, towards the proximal part of the delta, an intermediate resistivity zone Z2 (8200 to 39 000 Ωm , mean: 14 200) is present. In more distal areas the upper, high resistivity zone makes a sharp contact with either the low resistivity zone (Z3) (300 to 1550 Ωm , mean: 670 Ωm) or with zone Z4, which displays a wider range of resistivity responses (200 to 20 000 Ωm , mean 10 050 Ωm) (Fig. 14).

Outcrops and borehole profiles indicate that clay content is low. This is typical for well-sorted glaciofluvial and deltaic sediments (Glückert, 1986; Palmu, 1999; Zielinski & Loon, 2003; Winsemann *et al.*, 2018; Kurjanski *et al.*, 2020). Based on the geomorphology of the deltas, together with the available outcrops and GPR data, Z1 is interpreted as well-sorted, unsaturated (dry) sands and gravels (Fig. 13). Of note are the extremely high resistivity values, exceeding typical values for glacial sand and gravels (e.g. Palacky, 1988) but consistent within values detected from glacial sediments deposited by the Laurentide ice sheet (Culley *et al.*, 1976) and the Fennoscandian ice sheet in Finland (Sutinen, 1992). Such values are attributed to air-filled pore spaces within the sediments suggesting high permeability and rapid drainage above the water table.

The intermediate zone (Z2) is interpreted as either ice-proximal facies or a heterolithic sandy-silty package deposited in the distal part of the delta (Fig. 13). In comparison to Z1, the lower resistivity values most likely reflect poorer sorting resulting in higher water saturation and locally, lower porosity.

The lowest resistivity values are recorded in the saturated zone Z3, located beneath Z1, but are relatively high when compared to typical freshwater aquifers found in unconsolidated sandy sediments (e.g. Choudhury *et al.*, 2001; Batayneh, 2006; Galazoulas *et al.*, 2015). However, mineralization in water samples shows electrical conductivity values as low as 0.001 S m^{-1} (mean 0.016 S m^{-1}) (Table 3), which is consistent with meteoric water recharging the aquifer and short water retention times. The contrast between Z1 and Z3 is three or four orders of magnitude. In such areas

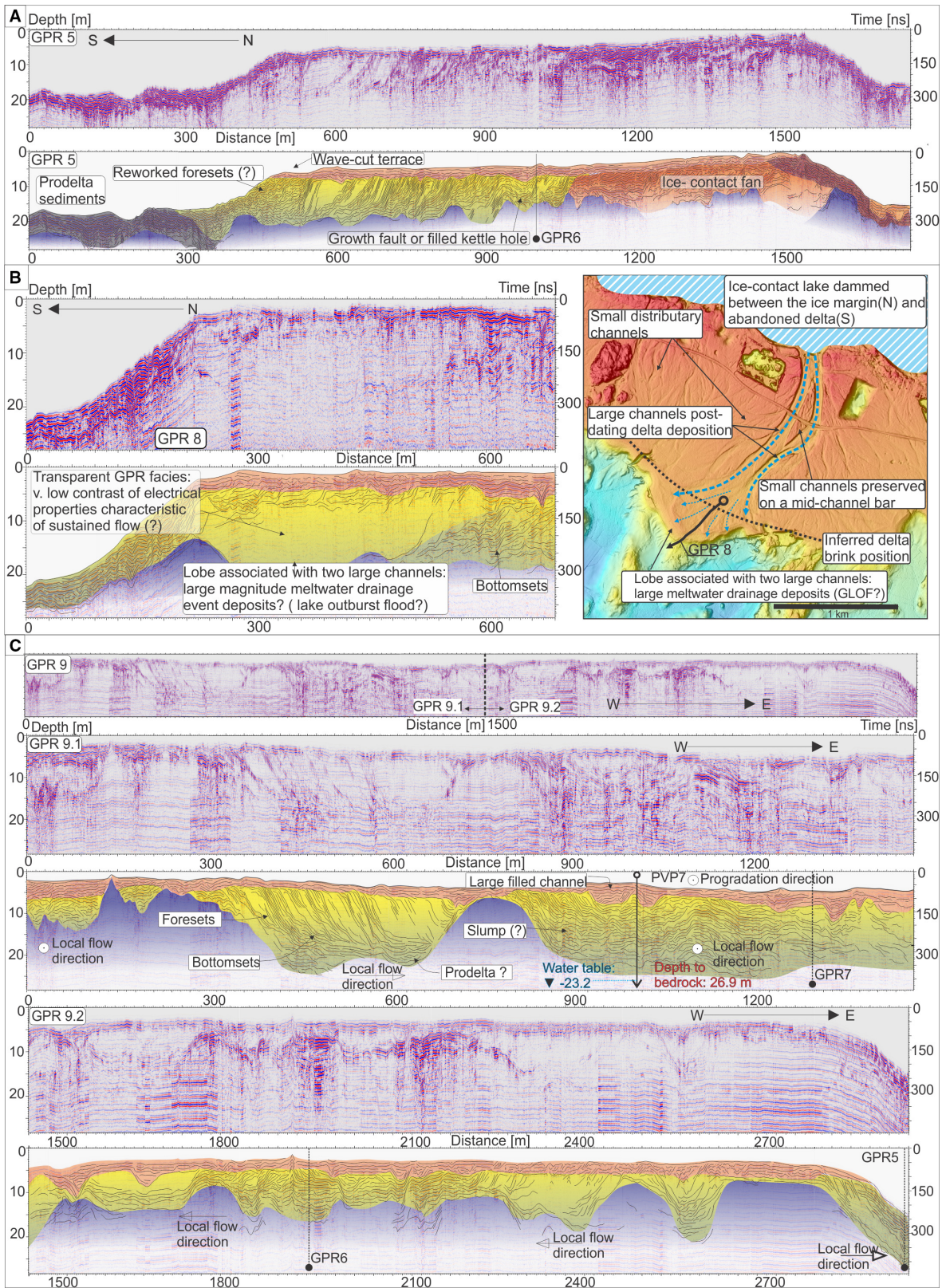


Fig. 10. See next page for figure caption.

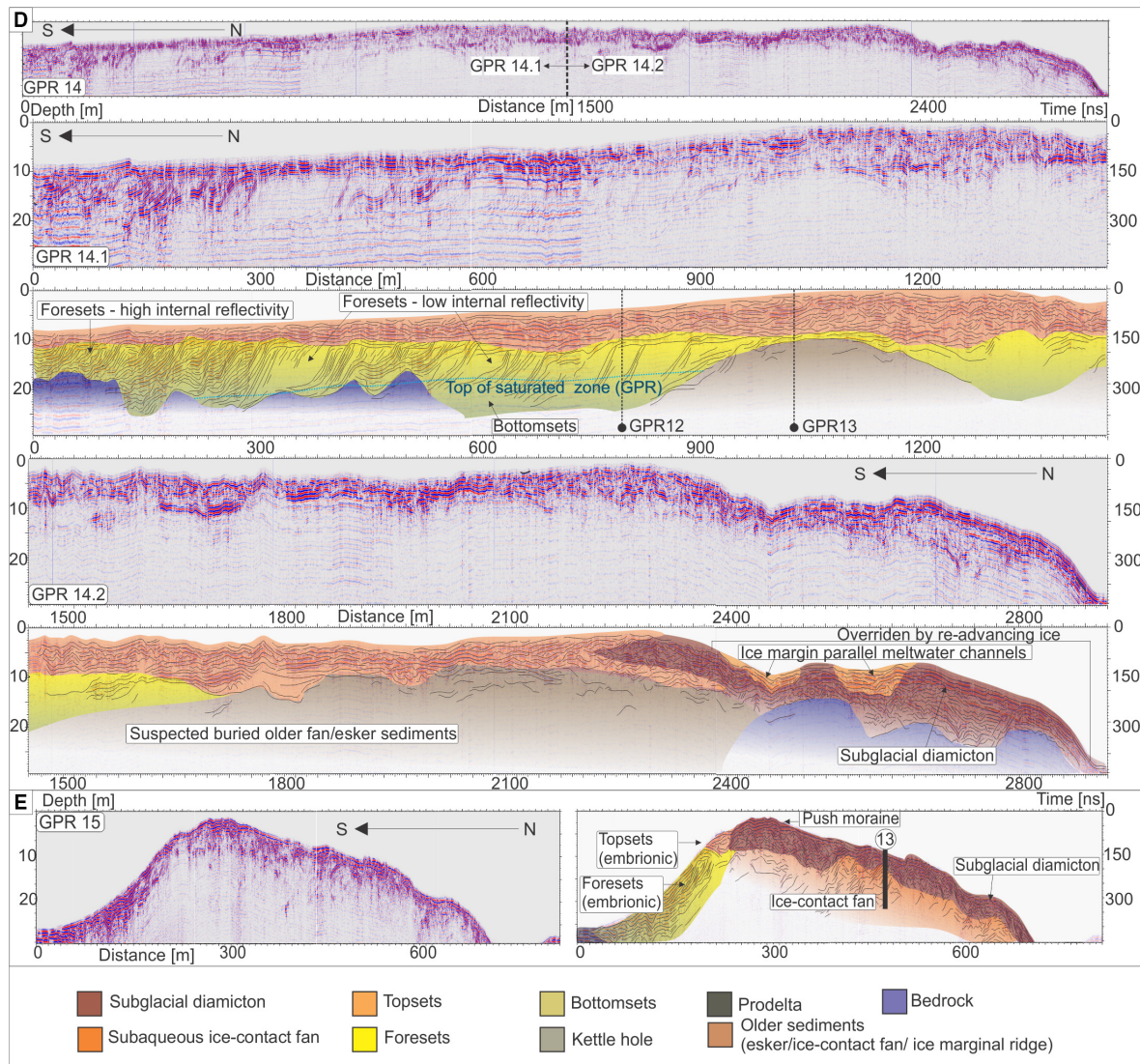


Fig. 10. Ground penetrating radar profiles (GPR) with interpretations. For locations see Fig. 3. For GPR profiles 1, 2, 3, 4, 6, 7, 10, 11, 12 and 13, see Appendix S1. Average relative dielectric permittivity (RDP) value of 6.2 was used for time-depth conversion.

the top of the saturated zone, rather than top of the bedrock, is likely to be imaged. It is important to note that average resistivity values for Z3 vary between ERT profiles. In profiles ERT1 and ERT2 the average resistivity is between 1100 to 1500 Ωm (minimum 675 Ωm) whereas in profile ERT3 the average is 801 Ωm (minimum 306 Ωm) (Fig. 14). None of the boreholes along these profiles encountered the water table. Bedrock elevation derived from gravity and borehole data located in the vicinity of the profile ERT 3 data suggests that an aquifer is only locally developed in hollows where the bedrock is over-deepened. This suggests that

water saturation is below 100% in most of the zone Z3 as infiltrating meteoric waters are in transit towards the underlying bedrock. Zone Z4 is characterized by a more variable resistivity response and interpreted as bedrock, based on the correlation to exposures (Fig. 7A and E).

Porosity determination from ERT

Data from Table 3 were used to calculate porosity within each zone (Z1 to Z3) (Table 3) (Fig. 14). Only areas above the depth of investigation (DOI) limit were considered. The porosity modelled for

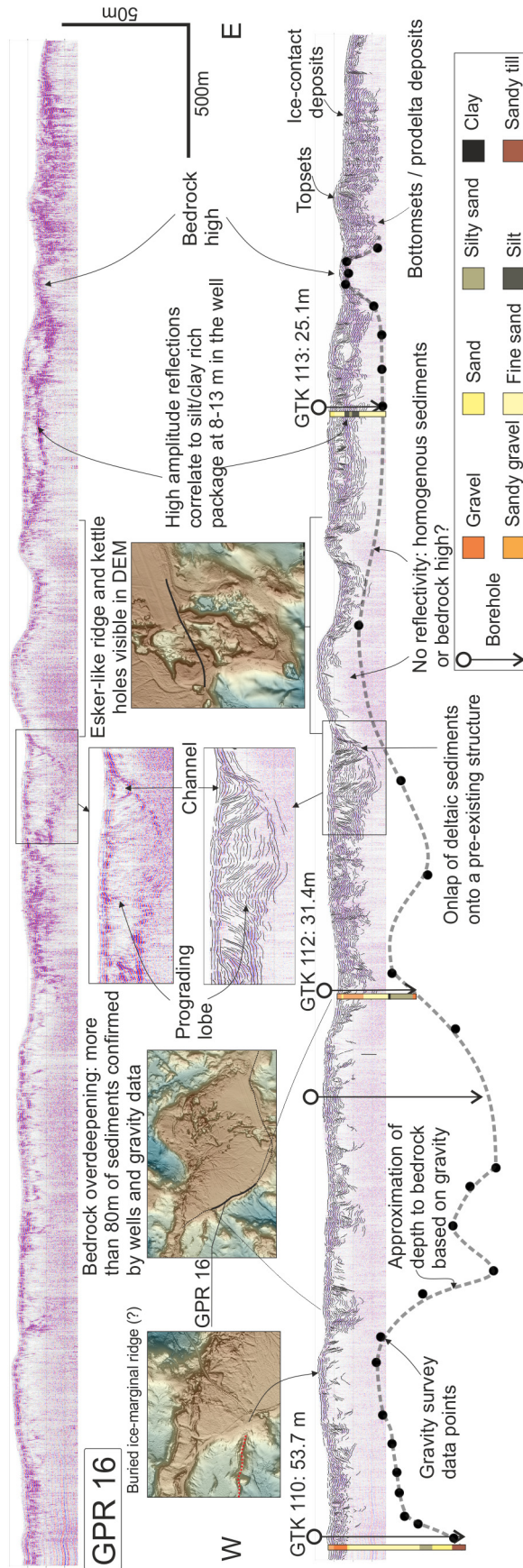


Fig. 11. Ground penetrating radar profile 16 with interpretation and correlated with boreholes. For profile location see Fig. 3. Note relatively shallow penetration depth of 100 MHz antenna when compared to the gravity data and large variations of sediment thickness.

zone Z1 is between 20% and 30% with extreme values bordering 40% (high) and 15% (low). Such a range is comparable to values reported from unconsolidated glaciofluvial sediments elsewhere (e.g. Olanrewaju & Wong, 1984; Salem, 2001a). It was assumed, based on the interpretation of the GPR profiles and sedimentary logs, that the difference in resistivity between zones Z1 and Z3 is mainly controlled by changes in water saturation rather than porosity. The only expected change is a decrease towards the bottom of the succession as a consequence of the increased fine fraction in the bottomset beds. Assuming the water saturation controls provided constraints for modelling the porosity of zone Z1 and Z3. Modelling of Z3 assumed 95% water saturation to account for a fully saturated aquifer and a transition zone, where saturation increases from close to 0% to 100%. Modelling returned porosity values between 10% and 20% for profiles ERT 1 and ERT 2, whereas in profile ERT 3 porosity of the saturated zone (Z3) ranges between 12.5% and 35%, with most of the values falling between 15% and 25% (Fig. 14). As above, an aquifer is likely to be present only locally in ERT 3, which implies that the average saturation of Z3 is below 95% and likely to be much lower in ERT 1 and ERT 2 (Figs 13 and 14; Appendix S1). Porosity values in ERT 1 and ERT 2 are likely underestimated and only in ERT 3 is the calculated porosity closer to satisfying the conditions outlined above.

Porosity falls between 25% and 40% in Z2 with unrealistically high (>48%) and low values (<10%) (Fig. 14). This is attributed to the poorer sorting and larger grain-size variations which are responsible for the broader resistivity range. The unrealistically high porosity values obtained in Z2, >30 to 35%, can be explained by a number of possible (and additive) errors: (i) underestimated resistivity values in Z2 which could be attributed to the inversion producing smooth transitions rather than a well-defined geological unit; (ii) underestimated values for water saturation; and (iii) the presence of clays in Z2, which would result in Archie's model largely overestimating porosity. This is supported by the presence of a fine fraction in the Z2 sediment package, which would favour a higher water saturation due to poorer sorting as seen in outcrop (Figs 6A, 6B, 8E, 8H, 8I and 14).

Depth to bedrock

Estimation for the thickness of the sedimentary sequence was achieved by combining results

from gravity measurements and water borehole logs, provided by the Geological Survey of Finland, together with outcrop, GPR and ERT data (Fig. 13; Appendix S1). The interpretation was performed using a set of rules, outlined in Fig. S2. Areas where at least two, and preferably three, geophysical methods overlap were interpreted with the highest confidence. Uncertainty increased away from boreholes and in places where geophysical methods yield diverging results. Since the gravity profiles were not acquired along accessible routes (roads and paths) it was impossible to acquire co-linear ERT data, which precluded the possibility to invert the ERT and gravity data together (Fig. 3). The depth to bedrock, based on the gravity survey, was used to interpolate the approximate depth to bedrock along all three ERT profiles (Fig. 13; Appendix S1). The only relatively robust gravity measurements along the ERT profiles are where gravity profiles intersect the resistivity lines (Figs 3 and 13).

The thickness of the delta sediments along the ERT and gravity profiles is highly variable. Less than 5 m of glaciofluvial sediments are present over bedrock highs (Figs 7E, 10C and 13). In the central, flat-topped part of the delta, the thickness usually varies between 10 to 45 m, except for deep bedrock troughs, which most likely followed structural lineaments, where borehole data show sediment thicknesses in excess of 90 m (Figs 11 and 13). The geophysical surveys undertaken here and boreholes in the vicinity of ERT 3 indicate a sediment thickness of *ca* 30 m (Fig. 13).

DISCUSSION

Integration of geomorphology, sedimentology and geophysics

Sedimentological studies of Quaternary glacial deposits can be supplemented with geophysical methods and geomorphological mapping. Together these offer the advantage of linking 2D exposures and profiles to a 3D geomorphic expression of glacial landforms, which is rarely possible for ancient depositional systems. An iterative, down-stepping approach in terms of penetration depth and resolution, using more than one geophysical method, was found to be most effective when characterizing the ice-contact Salpausselkä deltas (Figs 13 and 15). Outcrops were logged and their position within

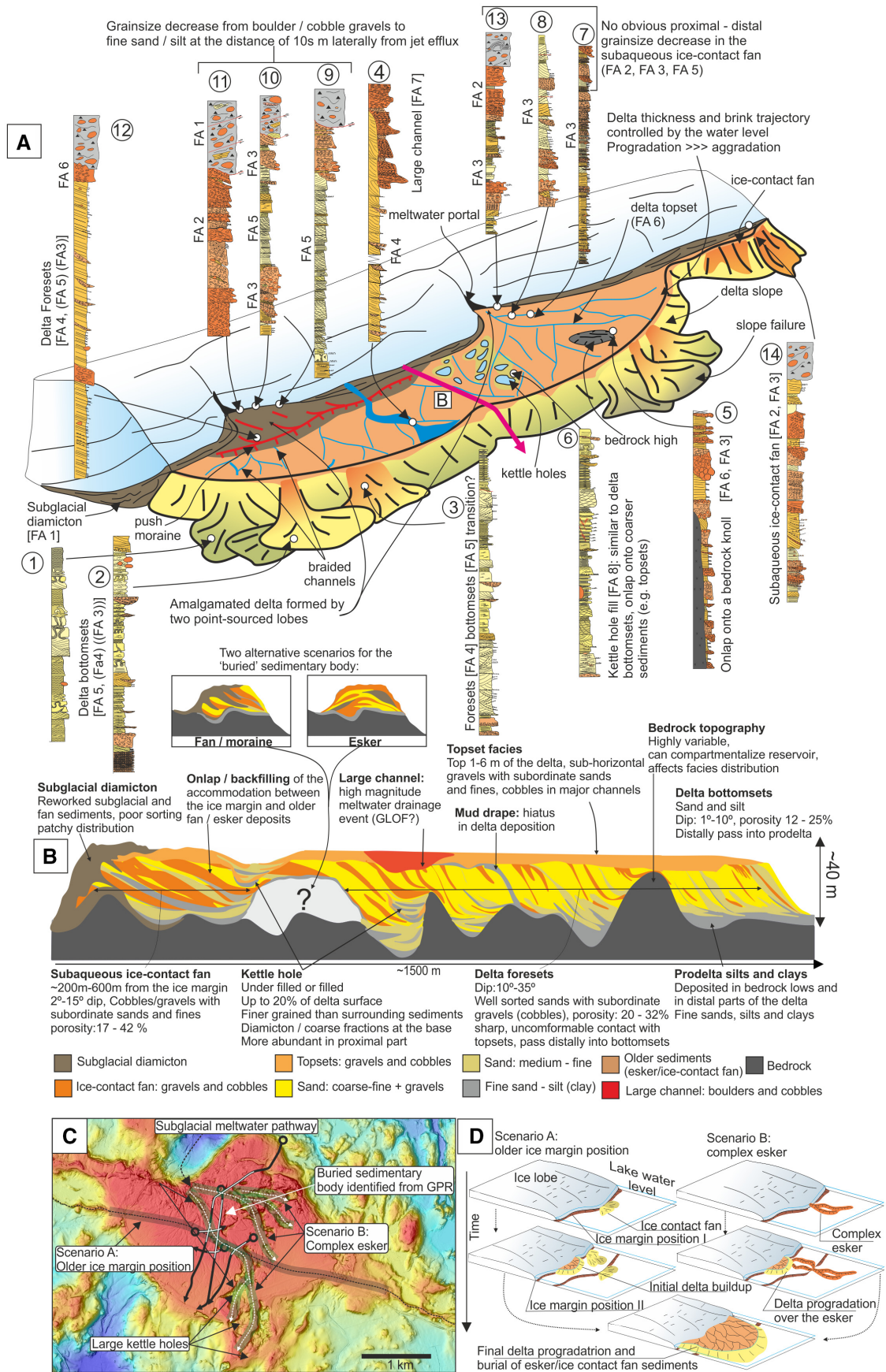


Fig. 12. Summary diagram showing: (A) an idealized ice-contact delta with locations of sedimentary logs with respect to their position within the delta based on geomorphology; (B) synthetic cross-section through an ice-contact delta. Modified from Gobo *et al.* (2015) and Lang *et al.* (2017). Note the large contrast in grain size, especially in the proximal part, and the role of bedrock and pre-existing sedimentary structures on facies distribution and potential fluid migration pathways. (C) and (D) Two conceptual models for the depositional history of Vesivhmaankangas (study area 2) based on interpretation of GPR and ERT profiles. For detailed sedimentary logs see Fig. 5, for their location see Fig. 2.

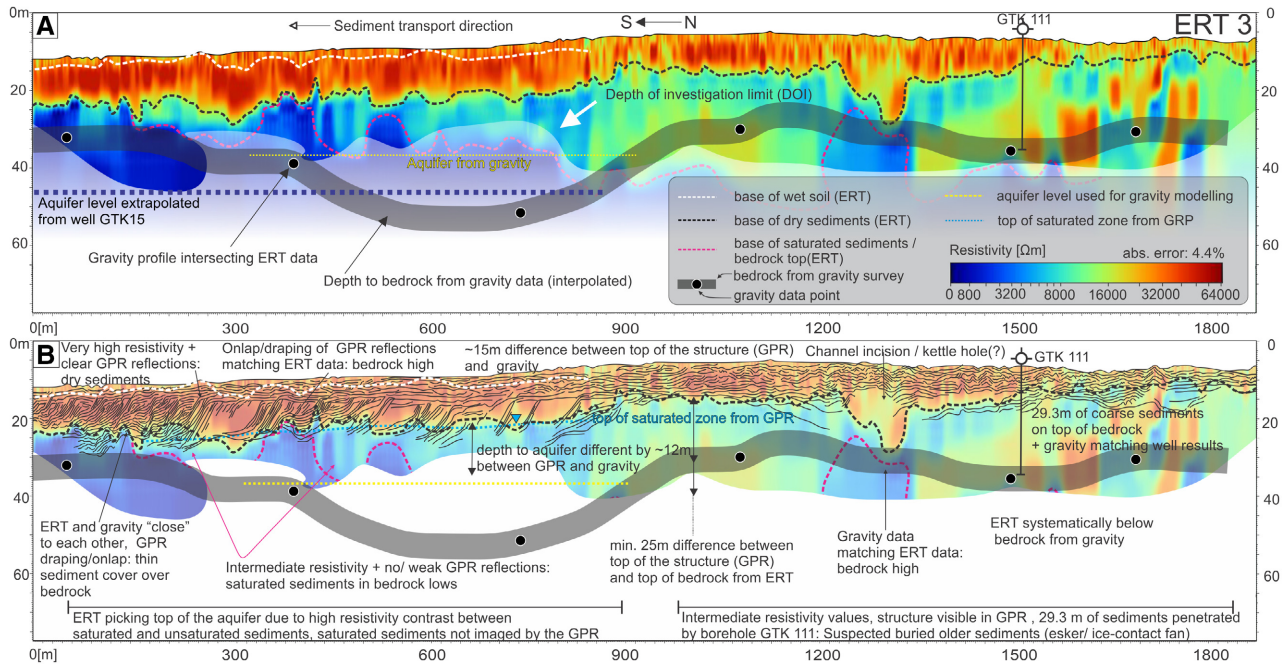


Fig. 13. Electrical resistivity tomography profiles: (A) profile ERT 3; (B) interpretation and corresponding GPR reflection pattern (Fig. 10D). For profiles ERT 1 and ERT 2 see Appendix S1. For location see Fig. 3.

the depositional system was identified using the morphological features observed from the LiDaR DEM (Fig. 2). GPR data was interpreted by linking reflection patterns to corresponding sediments observed in scarce exposures (Fig. 12). ERT and gravity methods were linked/overlapped with structures and sediments identified in the top 10 to 20 m from the GPR and exposures, which allowed extrapolation below the limit of GPR penetration (Figs 3, 11, 13 and 15). This approach provides the most robust interpretation of the sedimentary architecture of the Salpausselkä deltas.

Comparison of geophysical methods

The GPR is invaluable for understanding the subsurface sedimentary architecture and the depth to bedrock. Its utility is limited by the

maximum penetration depth, which, in unsaturated sediments, is *ca* 20 m for a bistatic 80 MHz GPR antenna configuration (Figs 10 and 11). The penetration depth is reduced significantly when the sediments are saturated, and/or clays/silts are present (Fig. 10). Comparison of the ERT and GPR data show that mapping depth to bedrock, based on the loss of GPR signal, leads to an underestimation of the profile cross-sectional area by *ca* 50%, with concomitant effects for calculating sediment volumes (Fig. 15). In bedrock lows, especially in the saturated zone, ERT exhibits a large difference from the gravity data (Fig. 13). This is most likely a result of the ERT picking the top of the aquifer/saturated zone rather than the top of the bedrock (Fig. 15). This again leads to underestimation of the sediment volumes. An opposite relationship between ERT and gravity (ERT depth to bedrock

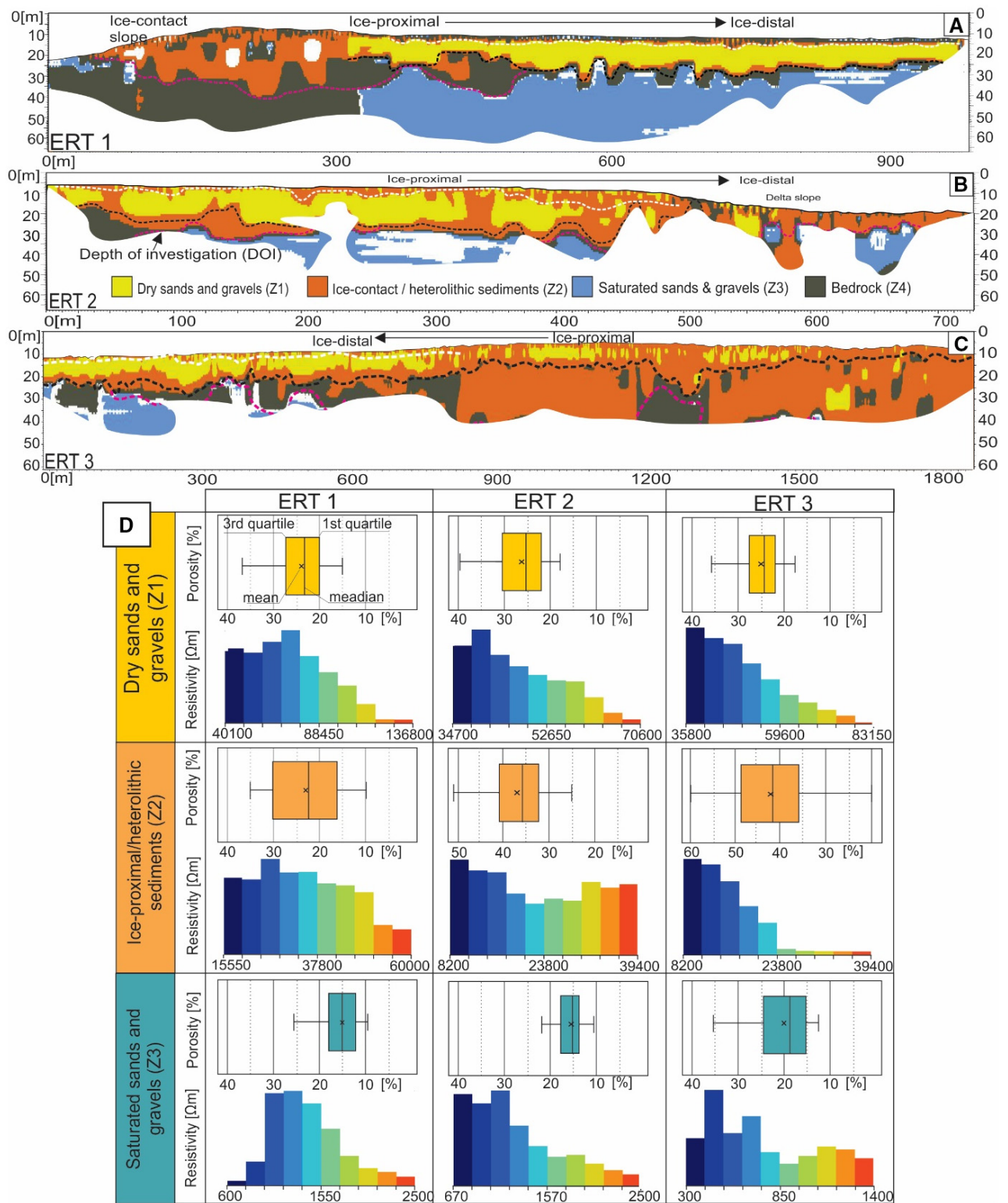
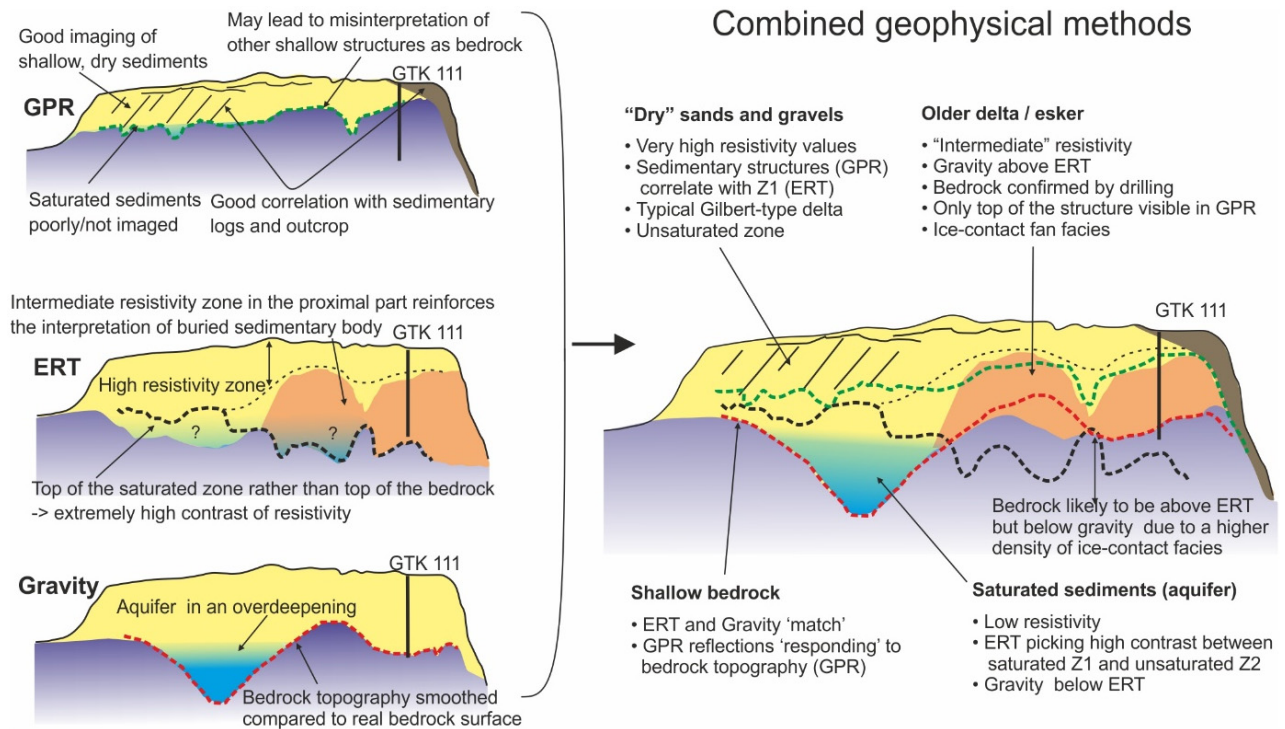


Fig. 14. Porosity distribution from ERT profiles. Each zone has been calculated using the parameters in Table 3: (A) profile ERT 1; (B) profile ERT 2; (C) profile ERT 3; and (D) frequency distribution of porosity and resistivity within each zone and profile.

Table 3. Parameters used for porosity calculation from ERT profiles.

Zone	Conductivity of water (C_w) [S/m] [*]		Cementation factor: (m) [†]		Water saturation: (S_w) [†]		Saturation Exponent: (n)	Porosity ϕ [%] ^{**}	
	Mean	SD	Mean	SD	Mean	SD		Mean	SD
Dry sands and gravels (Zone 1)	0.0161	0.0129	1.53	0.27	0.05	0.03	1.65 [§]		
Ice-proximal/heterolithic sediments (Zone 2)	0.0161	0.0129	1.53	0.27	0.1	0.03	1.65 [§]	35.8	5.5
Saturated sands and gravels (Zone 3)	0.0161	0.0129	1.53	0.27	0.95	0.03	2.00 [¶]		

^{*} From Geological Survey of Finland dataset: Kaivovesien laatu/The quality of well waters, JHS158:2005, ISO 19115:2005. [†] Calculated based on data from (Archie, 1942; Salem, 2001b; Glover, 2016; Byun *et al.*, 2019). [‡] Calculated through Monte Carlo simulation using average resistivity from each ERT profile and boundary condition: porosity Z1~ = porosity Z3 and matching mean resistivity value from all the profiles. [§] Best fit value for 'dry' sediments based on average resistivity within each zone and information from (Glover, 2017). [¶] Standard value for water saturated sands and sandstones (e.g. Archie, 1942; Glover, 2017). ^{**} Calculated based on data from (Olanrewaju & Wong, 1984; Salem, 2001b; Rose *et al.*, 2016).

**Fig. 15.** Comparison of geophysical methods used in this study.

< gravity depth to bedrock) can be seen mainly in ice-proximal settings (Fig. 13, Table S3). Borehole GTK111, which directly penetrates the section, shows a close correlation with the ERT result (Fig. 13). Gravity data, showing a

shallower depth to bedrock may be attributed to the density of the sediments, used as a parameter during gravity inversion. Proximal, ice-contact facies contain more coarse fractions (cobble and boulder) which may have an

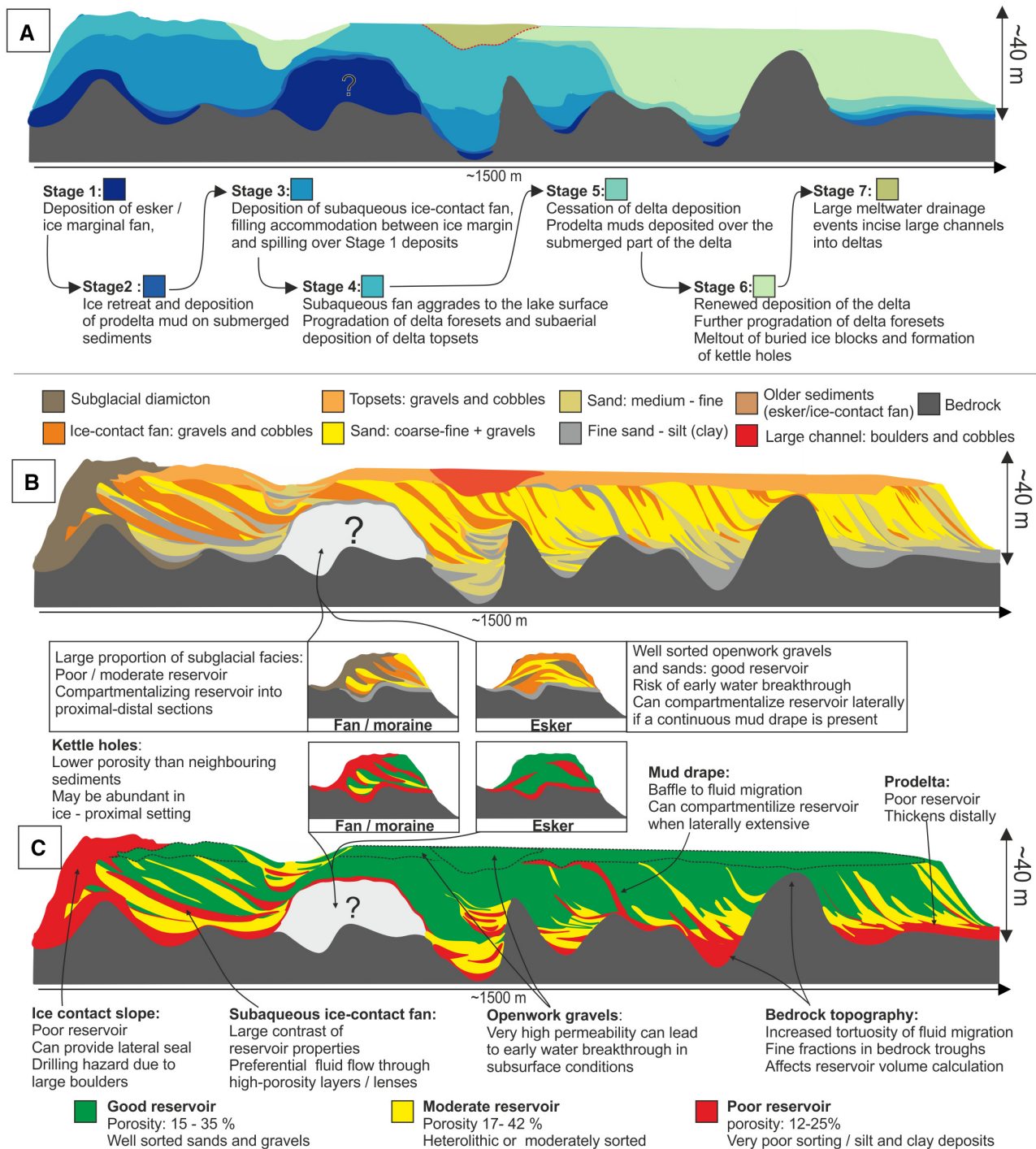


Fig. 16. (A) Relative timing of deposition for distinctive parts of the delta; and (B) a synthetic cross-section showing an idealized distribution of sediments within the ice-contact delta juxtaposed against (C) reservoir properties of sediments identified from outcrop studies and ERT survey.

intermediate (as a bulk) density between bedrock (high) and delta sediments (low). In these situations it may be beneficial to implement a four-layer model (dry delta sediments, proximal

fan sediments, water saturated sediments and bedrock) instead of the three-layer model used at present (dry sediments, saturated sediments and bedrock) to improve the gravity inversion.

Sedimentary facies distribution and their influence on reservoir properties

Gilbert-type deltas contain significant porous sedimentary bodies that are potential reservoirs for hydrocarbons, repositories for CO₂, sources of low enthalpy geothermal energy and aquifers (Knutsson, 2008; Arola *et al.*, 2014). Their sedimentology has been widely described and they are comprised of predictable facies successions (e.g. Gilbert, 1885; Mastalerz, 1990; Nemec & Postma, 1993; Lønne & Nemec, 2004; Rohais *et al.*, 2008; Colella & Prior, 2009; Gobo *et al.*, 2015; Chavarrías *et al.*, 2018; Winsemann *et al.*, 2018). The Salpausselkä I and II deltas are reliable water reservoirs (Figs 12 and 16) (Fyfe, 1990; Palmu, 1999; Maries *et al.*, 2017; Virtasalo *et al.*, 2019) and the porosity modelling in the current study has suggested that they have porosities within the 20 to 35% range, similar to values reported for other glaciofluvial deposits (Figs 14 and 16) (Olanrewaju & Wong, 1984; Salem, 2001b). Porosity appears to decrease towards the base of the delta (10 to 25% – Figs 14 and 16) due to the smaller grain size of the delta bottomsets/prodelta sediments. The presence of finer grained and/or poorly sorted slump deposits may decrease the reservoir quality further (Fig. 6A and B).

However, the reservoir performance of ice-contact deltas can be negatively affected by meso-scale heterogeneities which are directly linked to the depositional processes taking place at the ice margin (e.g. Mitten *et al.*, 2020). Evidence for ice overriding, bulldozing and mixing by ice-margin oscillations are clearly visible in delta morphology (Fig. 2). Eskers and ice marginal ridges observed in the topography on the trend of the deltas indicate that some of the older landforms might have been buried beneath them (Figs 2 and 12). Understanding of such complexities is crucial, especially for deeply buried or low-pressure reservoirs where relatively small changes in porosity/permeability properties can hugely affect the fluid flow.

In ice-proximal environments most of the deposition is associated with highly dynamic point-sourced discharge from subglacial and englacial conduits (Fig. 16). This leads to large, sharp and instantaneous (in geological terms) changes in sediment grain size (boulder gravel to very fine silt) occurring over short distances in all dimensions (x, y, z) and is reflected in the modelled porosity values, ranging from 10% to over 40% in in subaqueous ice-proximal fan

facies (Fig. 16) (Rust & Romanelli, 1975; Powell, 1990; Russell & Arnott, 2003). High porosity contrasts can lead to generation of ‘thief zones’ which are important when a two-phase flow (gas–liquid/water–oil) is considered, since they may lead to early water breakthrough in wells and isolation of gas pockets, effectively making production impossible (Li *et al.*, 2016; Satter & Iqbal, 2016). Glaciotectonic modification due to ice-margin oscillations may effectively decrease sorting of the ice-contact slope and therefore reduce porosity/permeability creating a zone of decreased reservoir potential (Fig. 16). Most subglacial diamictons (traction tills) are poorly sorted (mechanically mixed) with a fine-grained matrix, including substantial amounts of clay/clay sized material, resulting in low porosity and permeability, making them reasonably good seals (Benn & Evans, 1996; Evans *et al.*, 2006). This is only partially true for the study area since the tills in the region have, dominantly, a silty/fine sand matrix as their provenance is crystalline bedrock. The till is sandy and gravel-rich, locally clast-supported as a result of the cannibalization of glaciofluvial deltaic sediments (Fig. 8H and I). This part of the delta is a waste zone (a lower porosity–permeability, non-producing zone within a reservoir) rather than a seal capable of retaining a build-up of fluid pressure (Fig. 16).

Typically, deltas prograde into the basin with younger sediments deposited distally away from the efflux point (portal), resulting in proximal–distal younging. This rule does not always hold within ice-contact deltas because, in some cases, backstepping of the ice margin creates accommodation (lake) between the ice margin and previously deposited fan/delta deposits, moraines or eskers (Figs 10D, 12C, 12D and 16) (Ashley, 2002). This space may then be partially, or fully, infilled with younger delta deposits. The older delta may be then re-activated and overtopped, following which progradation further into the basin is re-established (Figs 12 and 16). A lacustrine mud drape covering older deltaic deposits is likely to be deposited in the time between the ice retreat and renewed delta progradation. When such a lake becomes overfilled and/or a significant lake level fall occurs creating a large gradient between two water bodies a large meltwater drainage event may take place. This is observed from the Hyrtiälänkan-gas Delta, where two large erosional meltwater channels incise the delta topset and feed a small forced regressive delta lobe which can be

identified because it lacks the distinctive internal reflectivity in GPR data, that is typical for bottomsets/distal delta settings elsewhere (Figs 2, 10B, 12 and 16). Geomorphology of the delta shows that the drainage channel incised the ice-proximal part of the delta whereas little or no incision occurred in the ice-distal slope. This suggests that at this location fill-and-spill model for lake drainage is more likely than the Baltic ice level fall scenario (Fig. 10A). Such erosional reworking of the delta topsets may deposit good reservoir quality sediments in bottomset or prodelta areas, which typically have moderate/poor reservoir properties (Fig. 16).

Kettle holes are clearly visible on the delta surface (Fig. 2) (Okko, 1962; Donner, 1976, 1995; Fleisher, 1986; Wingfield, 1990). When infilled and buried, kettle holes may introduce additional heterogeneities into the reservoir. The sediments filling the depressions are likely to be finer grained and of moderate/poor reservoir quality in comparison to surrounding topset, fan or foreset facies (good reservoirs) (Fig. 16). Kettle holes effectively decrease the total volume of the reservoir, their interpretation from well data (for example, based on palynology) may erroneously indicate a thinner reservoir package or a sandy transgressive package deposited on top of the deltas.

The dynamic nature of ice-contact deposition is likely to juxtapose sediments, which would not be in contact in non-glacial deltaic settings (for example, mud drape, esker sediments buried within delta bottomsets, subglacial diamicton above delta topsets and kettle holes) which introduces large contrasts in porosity and permeability to the reservoir (Fig. 16). This can be magnified when the deltas are buried or when reservoir pressures are relatively low, such as in the glaciogenic Pleistocene sediments of the North Sea (Le Heron *et al.*, 2006; Hirst, 2012; Martin *et al.*, 2012; Ottesen *et al.*, 2012; Rose *et al.*, 2016; Kurjanski *et al.*, 2020).

The underlying bedrock topography strongly influences the sediment distribution and reservoir properties of ice-contact deltas by deflecting or focusing meltwater flow which affects facies distribution (Fig. 16). The topography may also subdivide the reservoir, creating disconnected aquifers with independent water tables (buried lakes), or lengthen water migration and retention time reflecting the highly tortuous infiltration path taken to bypass bedrock highs (Figs 15 and 16). This is especially important for reservoir management, and heat transfer in geothermal

systems but also for evaluation of deeper reservoirs where the bedrock may not be accurately imaged, leading to errors in volume calculations and overestimations of connectivity.

CONCLUSIONS

In this study the ice-contact deltas of Salpausselka I and II, associated with the Younger Dryas Stadial stillstand of the Fennoscandian ice sheet, were investigated using a combination of geomorphology, sedimentology and geophysical surveys (ERT, GPR and gravity) to provide a full-spectrum evaluation of the ice-contact delta internal structure and reservoir properties and reservoir potential.

High and fluctuating discharge energy from meltwater portals was responsible for the deposition of subaqueous ice-contact fans under highly supercritical flow conditions depositing boulder to cobble sized clasts proximal to the ice margin with large cyclic steps and hydraulic jump deposits downflow. Ice-proximal deposits exhibit the highest grain-size variation distally and laterally. When the fans aggraded to the lake surface, progradation of steep (10 to 35°) delta foresets commenced, often leading to the coalescence of two or more neighbouring deltas. Deposition on such steep slopes was likely dominated by supercritical flow conditions (formation of cyclic steps and antidunes) which eventually decelerated and deposited finer fractions in the subcritical flow regime as bottomsets. The foresets were capped by subaerially deposited sandur-like coarse glaciofluvial topsets. Short-term fluctuations of the Baltic ice lake level resulted in incision and re-mobilization of parts of the foreset package (lake level fall) supplying coarse sediments to the distal part of the delta or flooding parts of the delta (lake level rise) changing the foreset stacking pattern from progradation to progradation/aggradation.

Overall, ice-contact deltas are excellent reservoirs (porosity 10 to 42%) but, except for the largest of deltas (Figs 2B and 4), they are rarely big enough to constitute a stand-alone exploration target. Alternatively, exploration of multiple, clustered deltas/fans may be economically viable. Their recognition in the subsurface largely depends on a good understanding of the depositional environment and/or illumination of permeable deposits by gas. Their structure is likely to be more complex than that of a typical Gilbert-type delta (Figs 12 and 16). This mainly

results from ice-marginal oscillations affecting sedimentation in the ice-proximal part of the delta and the typical temporally varying (diurnal to annual) magnitude of meltwater and sediment flux. Moreover, backstepping of the ice margin (almost instantaneous in geological terms) rearranges sediment input points and provides accommodation space 'behind' or laterally from a previously deposited delta, ice-contact fan or esker (Figs 2 and 12) (Ashley, 2002). This can result in complex, amalgamated deltas with 'hidden' heterogeneities buried within, and abrupt lateral and distal facies changes affecting overall reservoir potential (Figs 2 and 16). The localized presence of highly permeable zones or layers ('thief zones') can lead to preferential fluid flow through those zones and bypass of lower porosity/permeability and early water breakthrough in hydrocarbon producing wells. This may have a significant effect when gas production is considered, especially from shallow gas targets, where formation pressures are low, or in deeper targets, where compaction and cementation may amplify porosity-permeability heterogeneities. Finally, this study shows that sediment distribution is significantly affected by the subglacially-sculpted bedrock topography (Fig. 16). These deltas were deposited over an extremely variable bedrock topography with sediment thickness varying between zero metres, where bedrock highs outcrop at the delta surface, to over 90 m in bedrock troughs. Such an interplay between topography and deposition will likely reroute sediments leading to the development of a complex facies pattern.

Results of this work are relevant for both the aquifer and low enthalpy geothermal energy exploitation in the region as well as similar deposits in the subsurface associated with Pleistocene and pre-Pleistocene glacial periods, where commercially important reserves of water or hydrocarbons may exist.

ACKNOWLEDGEMENTS

We would like to thank Mariusz Miśkiewicz, Markus Valkama and Alekski Tuunainen for their help and company during the fieldwork. Hard work becomes much more enjoyable when there are good people around to share the burden. We are also grateful for the help and support provided by the team at the Geological Survey of Finland Espoo Office without whom this work

would have not been possible. Authors are very grateful for the constructive comments and suggestions offered by two anonymous reviewers which allowed us to greatly improve the manuscript. Least but not last, we would like to thank the editorial board of *Sedimentology*, Dr Victoria Valdez, Dr Ian Kane and Elaine Richardson for their prompt and efficient handling of the manuscript in times when none of the above should be taken for granted.

DATA AVAILABILITY STATEMENT

The data that support the findings of this study are available from the corresponding author upon reasonable request.

REFERENCES

- Aber, J.S., Croot, D.G. and Fenton, M.M. (1989) Small Composite-Ridges. *Glaciolact. Landform. Struct.*, 47–69.
- Ahonen, J., Ojalainen, J. and Valjus, T. (2011) Investigation of the geological structure of the groundwater area in the Vesivehmaankangas research area. Geological Survey of Finland Report, 21 pp.
- Alexander, J., Bridge, J.S., Cheel, R.J. and Leclair, S.F. (2001) Bedforms and associated sedimentary structures formed under supercritical water flows over aggrading sand beds. *Sedimentology*, **48**, 133–152.
- Andersen, T.R., Huuse, M., Jorgensen, F. and Christensen, S. (2012) Seismic investigations of buried tunnel valleys on- and offshore Denmark. *Geol. Soc., London, Spec. Public.*, **368**, 129–144
- Anderson, M.P. (1989) Hydrogeologic facies models to delineate large-scale spatial trends in glacial and glaciofluvial sediments. *Geol. Soc. Am. Bull.*, **101**, 501–511.
- Archie, G.E. (1942) The electrical resistivity log as an aid in determining some reservoir characteristics. *Trans. AIME*, **146**, 54–62.
- Arola, T., Eskola, L., Hellen, J. and Korkka-Niemi, K. (2014) Mapping the low enthalpy geothermal potential of shallow Quaternary aquifers in Finland. *Geotherm. Energy*, **2**, 9.
- Artimo, A., Mäkinen, J., Berg, R.C., Abert, C.C. and Salonen, V.P. (2003) Three-dimensional geologic modeling and visualization of the Virtaankangas aquifer, southwestern Finland. *Hydrogeol. J.*, **11**, 378–386.
- Ashley, G.M. (2002) 11 - Glaciolacustrine environments. In: *Modern and Past Glacial Environments* (Eds John Menzies, Modern and Past Glacial Environments and Butterworth-Heinemann), pp. 335–359. Amsterdam: Elsevier. <https://doi.org/10.1016/B978-075064226-2/50014-3>.
- Ashley, G.M., Southard, J.B. and Boothroyd, J.C. (1982) Deposition of climbing-ripple beds: a flume simulation. *Sedimentology*, **29**, 67–79.
- Backert, N., Ford, M.A. and Malartre, F. (2010) Architecture and sedimentology of the Kerinitis Gilbert-type fan delta, Corinth Rift, Greece. *Sedimentology*, **57**, 543–586.
- Barrett, B.J., Gawthorpe, R.L., Collier, R.E.L., Hodgson, D.M. and Cullen, T.M. (2020a) Syn-rift delta interfan

- successions: Archives of sedimentation and basin evolution. *Depos. Rec.*, **6**, 117–143.
- Barrett, B.J., Hodgson, D.M., Jackson, C.A.L., Lloyd, C., Casagrande, J. and Collier, R.E.L.** (2020b) Quantitative analysis of a footwall-scarp degradation complex and syn-rift stratigraphic architecture, Exmouth Plateau, NW Shelf, offshore Australia. *Basin Res*, **33**(2), 1135–1169.
- Bataller, F.J., McDougall, N. and Moscariello, A.** (2019) Ordovician glacial paleogeography: Integration of seismic spectral decomposition, well sedimentological data, and glacial modern analogs in the Murzuq Basin, Libya. *Interpretation*, **7**, T383–T408.
- Batayneh, A.T.** (2006) Use of electrical resistivity methods for detecting subsurface fresh and saline water and delineating their interfacial configuration: A case study of the eastern Dead Sea coastal aquifers, Jordan. *Hydrogeol. J.*, **14**, 1277–1283.
- Bendixen, M., Iversen, L.L. and Overeem, I.** (2017) Greenland: Build an economy on sand. *Science*, **358**, 879.
- Bendixen, M., Overeem, I., Rosing, M.T., Bjørk, A.A., Kjær, K.H., Kroon, A., Zeitz, G. and Iversen, L.L.** (2019) Promises and perils of sand exploitation in Greenland. *Nat. Sustain.*, **2**, 98–104.
- Benn, D.I. and Evans, D.J.A.** (1996) The interpretation and classification of subglacially-deformed materials. *Quat. Sci. Rev.*, **15**, 23–52.
- Benn, D.I. and Evans, D.J.A.** (2010) *Glaciers and Glaciation*, 2nd edn. Hodder Education, London, 802 pp.
- Bennett, M.R.** (2001) The morphology, structural evolution and significance of push moraines. *Earth Sci. Rev.*, **53**, 197–236.
- Bennett, M.R., Doyle, P. and Mather, A.E.** (1996) Dropstones: Their origin and significance. *Palaeogeogr. Palaeoclimatol. Palaeoecol.*, **121**, 331–339.
- Best, A., Arnaud, E., Parker, B., Aravena, R. and Dunfield, K.** (2015) Effects of glacial sediment type and land use on nitrate patterns in groundwater. *Groundw. Monit. Remediat.*, **35**, 68–81.
- Bjorck, S. and Digerfeldt, G.** (1984) Climatic changes at Pleistocene/ Holocene boundary in the Middle Swedish endmoraine zone, mainly inferred from stratigraphic indications. Climatic Changes on a Yearly to Millennial Basis. *Proc. 2nd Nord. Symp. Stock.*, **1983**, 37–56.
- Brandes, C., Polom, U. and Winsemann, J.** (2011) Reactivation of basement faults: interplay of ice-sheet advance, glacial lake formation and sediment loading. *Basin Res.*, **23**, 53–64.
- Breilin, O., Paalijärvi, M. and Valjus, T.** (2005) Investigation of the geological structure of the groundwater area at Asikkala Hyrtiälänkangas II in Salpausselä. Geological Survey of Finland Report, 16 pp.
- Breilin, O., Paalijärvi, M. and Valjus, T.** (2006) Investigation of the geological structure of the groundwater area at Asikkala Hyrtiälänkangas II in Salpausselä. Geological Survey of Finland Report, 17 pp.
- Brookfield, M.E. and Martini, I.P.** (1999) Facies architecture and sequence stratigraphy in glacially influenced basins: Basic problems and water-level/glacier input-point controls (with an example from the Quaternary of Ontario, Canada). *Sediment. Geol.*, **123**, 183–197.
- Burke, M.J., Brennand, T.A. and Sjogren, D.B.** (2015) The role of sediment supply in esker formation and ice tunnel evolution. *Quat. Sci. Rev.*, **115**, 50–77.
- Burke, M.J., Woodward, J. and Russell, A.J.** (2010) Sedimentary architecture of large-scale, jökulhlaup-generated, ice-block obstacle marks: Examples from Skeiðarárandsandur, SE Iceland. *Sediment. Geol.*, **227**, 1–10.
- Byun, Y.H., Hong, W.T. and Yoon, H.K.** (2019) Characterization of cementation factor of unconsolidated granular materials through time domain reflectometry with variable saturated conditions. *Materials (Basel)*, <https://doi.org/10.3390/ma12081340>.
- Carlson, A.E.** (2013) Paleoclimate | The younger dryas climate event. In: *Encyclopedia of Quaternary Science* (Eds Elias, S.A. and Mock, C.J.), 2nd edn, pp. 126–134. Elsevier B.V, Amsterdam. <https://doi.org/10.1016/B978-0-444-53643-3.00029-7>.
- Catuneanu, O.** (2006) *Principles of Sequence Stratigraphy*. Elsevier, 375 pp.
- Chavarrías, V., Blom, A., Orrú, C., Martín-Vide, J.P. and Viparelli, E.** (2018) A Sand-Gravel Gilbert Delta Subject to Base Level Change. *J. Geophys. Res. Earth Surf.*, **123**, 1160–1179.
- Choudhury, K., Saha, D.K. and Chakraborty, P.** (2001) Geophysical study for saline water intrusion in a coastal alluvial terrain. *J. Appl. Geophys.*, **46**, 189–200.
- Clague, J.J. and Evans, S.G.** (2000) A review of catastrophic drainage of moraine-dammed lakes in British Columbia. *Quat. Sci. Rev.*, **19**, 1763–1783.
- Colella, A. and Prior, D.B.** (2009) *Coarse-Grained Deltas*. Wiley Blackwell, Oxford, pp. 1–357.
- Comte, J.C., Cassidy, R., Nitsche, J., Ofterdinger, U., Pilatova, K. and Flynn, R.** (2012) The typology of Irish hard-rock aquifers based on an integrated hydrogeological and geophysical approach. *Hydrogeol. J.*, **20**, 1569–1588.
- Covault, J.A., Kostic, S., Paull, C.K., Sylvester, Z. and Fildani, A.** (2017) Cyclic steps and related supercritical bedforms: Building blocks of deep-water depositional systems, western North America. *Mar. Geol.*, **393**, 4–20.
- Culley, R.W., Jagodits, F.L. and Middleton, R.S.** (1976) E-phase system for detecting buried granular deposits. *Transp. Res. Rec.*, 1–10.
- Demidov, I., Houmark-Nielsen, M., Kjær, K. and Larsen, E.** (2006) The last Scandinavian Ice Sheet in northwestern Russia: Ice flow patterns and decay dynamics. *Boreas*, **35**, 425–443.
- Dietrich, P., Ghienne, J.-F., Normandeau, A. and Lajeunesse, P.** (2016) Upslope-migrating bedforms in a proglacial sandur delta: Cyclic steps from river-derived underflows? *J. Sediment. Res.*, **86**, 113–123.
- Dietrich, P., Ghienne, J.-F., Schuster, M., Lajeunesse, P., Nutz, A., Deschamps, R., Roquin, C. and Düringer, P.** (2017a) From outwash to coastal systems in the Portneuf-Forestville deltaic complex (Québec North Shore): Anatomy of a forced regressive deglacial sequence. *Sedimentology*, **64**, 1044–1078.
- Dietrich, P., Ghienne, J.-F., Normandeau, A. and Lajeunesse, P.** (2017b) Reconstructing ice-margin retreat using delta morphostratigraphy. *Sci. Rep.*, **7**, 16936.
- Dietrich, P., Ghienne, J.-F., Lajeunesse, P., Normandeau, A., Deschamps, R. and Razin, P.** (2018) Deglacial sequences and glacio-isostatic adjustment: Quaternary compared with Ordovician glaciations. *Geol Soc London, Spec Publ.*, **475**, 149–179.
- Domack, E.W. and Lawson, D.E.** (1985) Pebble Fabric in an Ice-Rafted Diamict. *J. Geol.*, **93**, 577–591.
- Donner, J.J.** (1969) Land/sea level changes in southern Finland during the formation of the Salpausselkä endmoraines. *Bull. Geol. Soc. Finl.*, **41**, 135–150.
- Donner, J.** (1976) *Suomen kvartääriegerologia*. Helsingin Yliopisto, Helsinki, 60 pp.

- Donner, J.** (1995) *Quaternary History of Scandinavia*. Cambridge University Press, Cambridge, 200 pp.
- Donner, J.** (2010) The younger dryas age of the salpausselkä moraines in Finland. *Bull. Geol. Soc. Finl.*, **82**, 69–80.
- Dowdeswell, J.A., Hogan, K.A. and Le Heron, D.P.** (2019) The glacier-influenced marine record on high-latitude continental margins: Synergies between modern, Quaternary and ancient evidence. *Geol. Soc. Spec. Public. Geol. Soc. London*, **475**, 261–279.
- Ehlers, J., Gibbard, P.L. and Hughes, P.D.** (2011) *Quaternary Glaciations - Extent and Chronology: A Closer Look*. Elsevier, Oxford, 1108 pp.
- Erickson, M.L., Yager, R.M., Kauffman, L.J. and Wilson, J.T.** (2019) Drinking water quality in the glacial aquifer system, northern USA. *Sci. Total Environ.*, **694**, 133735.
- Eronen, M., Glückert, G. and Hatakka, L.** (2001) Rates of Holocene isostatic uplift and relative sea-level lowering of the Baltic in SW Finland based on studies on isolation contacts. *Boreas*, **30**, 17–30.
- Evans, D.J.A.** (2006) Glacial Landscapes. In: *Glacier Science and Environmental Change* (Ed. Knight, P.G.), pp. 83–88. Blackwell Publishing, Malden, MA.
- Evans, D.J.A., Ewertowski, M. and Orton, C.** (2017) The glaciated valley landsystem of morsárjökull, southeast Iceland. *J. Maps*, **13**, 909–920.
- Evans, D.J.A., Hiemstra, J.F. and Cofaigh, C.O.** (2012) Stratigraphic architecture and sedimentology of a Late Pleistocene subaqueous moraine complex, southwest Ireland. *J. Quat. Sci.*, **27**, 51–63.
- Evans, D.J.A., Phillips, E.R., Hiemstra, J.F. and Auton, C.A.** (2006) Subglacial till: Formation, sedimentary characteristics and classification. *Earth-Science Rev.*, **78**, 115–176.
- Evans, D.J.A., Twigg, D.R., Rea, B.R. and Orton, C.** (2009) Surging glacier landsystem of tungnaárjökull, iceland. *J. Maps*, **5**, 134–151.
- Fisher, T.G. and Smith, D.G.** (1993) Exploration for Pleistocene aggregate resources using process-depositional models in the Fort McMurray region, Ne Alberta, Canada. *Quat. Int.*, **20**, 71–80.
- Fleisher, P.J.** (1986) Dead-ice sinks and moats: environments of stagnant ice deposition. *Geology*, **14**, 39–42.
- Fyfe, G.J.** (1990) The effect of water depth on ice-proximal glaciolacustrine sedimentation: Salpausselkä I, southern Finland. *Boreas*, **19**, 147–164.
- Gabriel, G., Kirsch, R., Siemon, B. and Wiederhold, H.** (2003) Geophysical investigation of buried Pleistocene subglacial valleys in Northern Germany. *J. Appl. Geophys.*, **53**, 159–180.
- Galazoulas, E.C., Mertzanides, Y.C., Petalas, C.P. and Kargiotis, E.K.** (2015) Large scale electrical resistivity tomography survey correlated to hydrogeological data for mapping groundwater salinization: A case study from a multilayered coastal aquifer in Rhodope, northeastern Greece. *Environ. Process.*, **2**, 19–35.
- Galloway, W.E.** (1975) Process framework for describing the morphologic and stratigraphic evolution of deltaic systems. In: *Deltas: Models for Exploration* (Ed. Broussard, M.L.). Houston Geological Society, Houston, 555 pp.
- Ghienne, J., Normandeau, A., Dietrich, P., Bouysson, M., Lajeunesse, P. and Schuster, M.** (2021) The depositional signature of cyclic steps: A late Quaternary analogue compared to modern active delta slopes. *Sedimentology*, **68**, 1502–1538.
- Gilbert, G.K.** (1885) *The Topographic Features of Lake Shores*. U.S. Government Printing Office, Washington, 75–123 pp.
- Gilbert, G.K.** (1890) *Lake Bonneville, US Geological Survey Monograph*. US Government Printing Office, Washington, DC, 438 pp.
- Girard, F., Ghienne, J.F., Du-Bernard, X. and Rubino, J.L.** (2015) Sedimentary imprints of former ice-sheet margins: Insights from an end-Ordovician archive (SW Libya). *Earth-Sci. Rev.*, **148**, 259–289.
- Glover, P.W.J.** (2016) Archie's law - A reappraisal. *Solid Earth*, **7**, 1157–1169.
- Glover, P.W.J.** (2017) A new theoretical interpretation of Archie's saturation exponent. *Solid Earth*, **8**, 805–816.
- Glückert, G.** (1986) The First Salpausselkä at Lohja, southern Finland. *Bull. Geol. Soc. Finl.*, **58**, 45–55.
- Glückert, G.** (1995) The Baltic Ice Lake in south Finland and its outlets. *Quat. Int.*, **27**, 47–51.
- Gobo, K., Ghinassi, M. and Nemeč, W.** (2014) Reciprocal changes in foreset to bottomset facies in a gilbert-type delta: Response to short-term changes in base level. *J. Sediment. Res.*, **84**, 1079–1095.
- Gobo, K., Ghinassi, M. and Nemeč, W.** (2015) Gilbert-type deltas recording short-term base-level changes: Delta-brink morphodynamics and related foreset facies. *Sedimentology*, **62**, 1923–1949.
- Gomez, B., Smith, L.C., Magilligan, F.J., Mertes, L.A.K. and Smith, N.D.** (2000) Glacier outburst floods and outwash plain development: Skeiðarársandur, Iceland. *Terra Nov.*, **12**, 126–131.
- Götz, J., Salcher, B., Starnberger, R. and Krisai, R.** (2018) Geophysical, topographic and stratigraphic analyses of perialpine kettles and implications for postglacial mire formation. *Geogr. Ann. Ser. A. Phys. Geogr.*, **100**, 254–271.
- Gruszka, B., and van Loon, A.J.** (2007) Pleistocene glaciolacustrine breccias of seismic origin in an active graben (central Poland). *Sediment. Geol.*, **193**, 93–104.
- Gruszka, B., Morawski, W. and Zieliński, T.** (2012) Sedimentary record of a Pleistocene ice-sheet interlobate zone (NE Poland). *Geologos*, **18**, 65–81.
- Hage, S., Cartigny, M.J.B., Clare, M.A., Sumner, E.J., Vendettuoli, D., Clarke, J.E.H., Hubbard, S.M., Talling, P.J., Gwyn Lintern, D., Stacey, C.D., Englert, R.G., Vardy, M.E., Hunt, J.E., Yokokawa, M., Parsons, D.R., Hizzett, J.L., Azpiroz-Zabala, M. and Vellinga, A.J.** (2018) How to recognize crescentic bedforms formed by supercritical turbidity currents in the geologic record: Insights from active submarine channels. *Geology*, **46**, 563–566.
- Hartley, A.J., Weissmann, G.S., Nichols, G.J. and Warwick, G.L.** (2010) Large distributive fluvial systems: characteristics, distribution, and controls on development. *J. Sediment. Res.*, **80**, 167–183.
- Heinz, J., Kleineidam, S., Teutsch, G. and Aigner, T.** (2003) Heterogeneity patterns of Quaternary glaciofluvial gravel bodies (SW-Germany): Application to hydrogeology. *Sediment. Geol.*, **158**, 1–23.
- Hirst, J.P.P.** (2012) Ordovician proglacial sediments in Algeria: insights into the controls on hydrocarbon reservoirs in the In Amenas field, Illizi Basin. *Geol. Soc. London. Spec. Publ.*, **368**, 319–353.
- Hirst, J.P.P., Benbakir, A., Payne, D.F. and Westlake, I.R.** (2002) Tunnel valleys and density flow processes in the Upper Ordovician glacial succession, Illizi Basin, Algeria: Influence on reservoir quality. *J. Pet. Geol.*, **25**, 297–324.
- Hornung, J.J., Asprion, U. and Winsemann, J.** (2007) Jet-efflux deposits of a subaqueous ice-contact fan, glacial

- Lake Rinteln, northwestern Germany. *Sediment. Geol.*, **193**, 167–192.
- Howell, J.A., Skorstad, A., MacDonald, A., Fordham, A., Flint, S., Fjellvoll, B. and Manzocchi, T.** (2008) Sedimentological parameterization of shallow-marine reservoirs. *Pet. Geosci.*, **14**, 17–34.
- Hoyal, D.C.J.D., Van Wagoner, J.C., Adair, N.L., Deffenbaugh, M., Li, D., Sun, T., Huh, C. and Giffin, D.E.** (2003) Sedimentation from jets: A depositional model for clastic deposits of all scales and environments. *Search Discov. Artic.* #40082. http://www.searchanddiscovery.com/documents/vw_hoyal/
- Hughes, P.D. and Gibbard, P.L.** (2015) A stratigraphical basis for the Last Glacial Maximum (LGM). *Quat. Int.*, **383**, 174–185.
- Huuse, M., Le Heron, D.P., Dixon, R., Redfern, J., Moscariello, A. and Craig, J.** (2012) Glaciogenic reservoirs and hydrocarbon systems: an introduction. *Geol. Soc. London. Spec. Publ.*, **368**, 1–28.
- Hyttinen, O., Salonen, V.P. and Kaakinen, A.** (2011) Depositional evidence of water-level changes of the Baltic ice lake in southern Finland during the younger dryas/holocene transition. *GFF*, **133**, 77–88.
- Jantunen, T. and Donner, J.** (1996) The formation of raised beaches in southern Finland during the Ancyclus and Litorina stages. *Bull. Geol. Soc. Finl.*, **68**, 34–39.
- Johansson, P., Lunkka, J.P. and Sarala, P.** (2011) The glaciation of Finland. *Dev. Quat. Sci.*, **15**, 105–116.
- Kalm, V.** (2012) Ice-flow pattern and extent of the last Scandinavian Ice Sheet southeast of the Baltic Sea. *Quat. Sci. Rev.*, **44**, 51–59.
- Kessler, T.C., Klint, K.E.S., Nilsson, B. and Bjerg, P.L.** (2012) Characterization of sand lenses embedded in tills. *Quat. Sci. Rev.*, **53**, 55–71.
- Knight, J.** (2019) The geomorphology and sedimentology of eskers in north-central Ireland. *Sediment. Geol.*, **382**, 1–24.
- Knutsson, G.** (2008) Hydrogeology in the Nordic countries. *Episodes*, **31**, 148–154.
- Kostic, S., Casalbore, D., Chiocci, F., Lang, J. and Winsemann, J.** (2019) Role of upper-flow-regime bedforms emplaced by sediment gravity flows in the evolution of deltas. *J. Mar. Sci. Eng.*, **7**, 5.
- Kurjański, B., Rea, B.R., Spagnolo, M., Cornwell, D.G., Howell, J. and Archer, S.** (2020) A conceptual model for glaciogenic reservoirs: From landsystems to reservoir architecture. *Mar. Pet. Geol.*, **115**, 104205.
- Lajeunesse, P. and Allard, M.** (2002) Sedimentology of an ice-contact glaciomarine fan complex, Nastapoka Hills, eastern Hudson Bay, northern Québec. *Sediment. Geol.*, **152**, 201–220.
- Lang, J., Brandes, C. and Winsemann, J.** (2017a) Erosion and deposition by supercritical density flows during channel avulsion and backfilling: Field examples from coarse-grained deepwater channel-levee complexes (Sandino Forearc Basin, southern Central America). *Sediment. Geol.*, **349**, 79–102.
- Lang, J., Dixon, R.J., Le Heron, D.P. and Winsemann, J.** (2012) Depositional architecture and sequence stratigraphic correlation of Upper Ordovician glaciogenic deposits, Illizi Basin, Algeria. *Geol. Soc. London. Spec. Publ.*, **368**, 293–317.
- Lang, J., Le Heron, D.P., Van den Berg, J.H. and Winsemann, J.** (2021) Bedforms and sedimentary structures related to supercritical flows in glaciogenic settings. *Sedimentology*, **68**, 1539–1579.
- Lang, J., Sievers, J., Loewer, M., Igel, J. and Winsemann, J.** (2017b) 3D architecture of cyclic-step and antidune deposits in glaciogenic subaqueous fan and delta settings: Integrating outcrop and ground-penetrating radar data. *Sediment. Geol.*, **362**, 83–100.
- Le Heron, D.P., Craig, J., Sutcliffe, O.E. and Whittington, R.** (2006) Late Ordovician glaciogenic reservoir heterogeneity: An example from the Murzuq Basin, Libya. *Mar. Pet. Geol.*, **23**, 655–677.
- Lee, R.E., Maclachlan, J.C. and Eyles, C.H.** (2018) Landsystems of Morsárjökull, Skaftafellsjökull and Svínafellsjökull, outlet glaciers of the Vatnajökull Ice Cap, Iceland. *Boreas*, **47**, 1199–1217.
- Levson, V., Ferbey, T., Kerr, B., Johnsen, T., Bednarski, J., Blackwell, J., and Jonnes, S.** (2003) Quaternary geology and aggregate mapping in northeast British Columbia: applications for oil and gas exploration and development. In: *Summary of Activities 2004*, pp. 29–40. British Columbia Ministry of Energy, Mines and Petroleum Resources, Resource Development and Geoscience Branch, Victoria.
- Li, D., Yang, J. and Lu, D.** (2016) Thief zone identification based on transient pressure analysis: a field case study. *J. Pet. Explor. Prod. Technol.*, **6**, 63–72.
- Lin, W. and Bhattacharya, J.P.** (2020) Storm-flood-dominated delta: A new type of delta in stormy oceans. *Sedimentology*, **68**, 1109–1136.
- Lønne, I.** (1995) Sedimentary facies and depositional architecture of ice-contact glaciomarine systems. *Sediment. Geol.*, **98**, 13–43.
- Lønne, I. and Nemec, W.** (2004) High-arctic fan delta recording deglaciation and environment disequilibrium. *Sedimentology*, **51**, 553–589.
- van Loon, A.J.T., Pisarska-Jamroz, M., Nartišs, M., Krievāns, M. and Soms, J.** (2016) Seismites resulting from high-frequency, high-magnitude earthquakes in Latvia caused by Late Glacial glacio-isostatic uplift. *J. Palaeogeogr.*, **5**, 363–380.
- Lunkka, J.P., Palmu, J. and Seppänen, A.** (2020) Deglaciation dynamics of the Scandinavian Ice Sheet in the Salpausselkä zone, southern Finland. *Boreas*, **bor.12502**.
- Maizels, J.** (1977) Experiments on the origin of kettle-holes. *J. Glaciol.*, **18**, 291–303.
- Mäkinen, J. and Palmu, J.P.** (2008) Collapse of sediment-filled crevasses associated with floods and mass flows in the proximal zone of the Pernunnummi sandurdelta, III Salpausselkä, SW Finland. *Quat. Sci. Rev.*, **27**, 1992–2011.
- Maries, G., Ahokangas, E., Mäkinen, J., Pasanen, A. and Malehmir, A.** (2017) Interlobate esker architecture and related hydrogeological features derived from a combination of high-resolution reflection seismics and refraction tomography, Virttaankangas, southwest Finland. *Hydrogeol. J.*, **25**, 1–17.
- Marks, L.** (2012) Timing of the Late Vistulian (Weichselian) glacial phases in Poland. *Quat. Sci. Rev.*, **44**, 81–88.
- Marren, P.M.** (2005) Magnitude and frequency in proglacial rivers: a geomorphological and sedimentological perspective. *Earth-Science Rev.*, **70**, 203–251.
- Martin, J.R., Redfern, J. and Williams, B.P.J.** (2012) Evidence for multiple ice centres during the late Palaeozoic ice age in Oman: Outcrop sedimentology and provenance of the late Carboniferous-Early Permian Al Khilata Formation. *Geol. Soc. Spec. Publ.*, **368**, 229–256.
- Mastalerz, K.** (1990) Diurnally and seasonally controlled sedimentation on a glaciolacustrine foreset slope: an example from the pleistocene of Eastern Poland. In:

- Coarse-Grained Deltas* (Eds Colella, A. and Prior, D.B.), pp. 297–309. Blackwell Publishing Ltd., Oxford.
- Mitten, A.J., Mullins, J., Pringle, J.K., Howell, J. and Clarke, S.M.** (2020) Depositional conditioning of three dimensional training images: Improving the reproduction and representation of architectural elements in sand-dominated fluvial reservoir models. *Mar. Pet. Geol.*, **113**, 104156.
- Mossa, J. and James, L.A.** (2013) Impacts of mining on geomorphic systems, In: *Treatise on Geomorphology* (Eds James, A., Harden, C. and Clague, J.), Vol. **13**, pp. 74–95. Elsevier Inc, Amsterdam.
- Nemec, W., Lønne, I. and Blikra, L.H.** (2008) The Kregnes moraine in Gauldalen, west-central Norway: anatomy of a Younger Dryas proglacial delta in a palaeofjord basin*. *Boreas*, **28**, 454–476.
- Nemec, W. and Postma, G.** (1993) Alluvial sedimentation. *Alluv. Sediment.*, 235–276.
- Nironen, M.** (2017) Guide to the Geological Map of Finland - Bedrock 1:1000000. Geological Survey of Finland Special Paper 60, pp. 41–76.
- Nyberg, B. and Howell, J.A.** (2016) Global distribution of modern shallow marine shorelines. Implications for exploration and reservoir analogue studies. *Mar. Pet. Geol.*, **71**, 83–104.
- Ó Dochartaigh, B.E., MacDonald, A.M., Black, A.R., Everest, J., Wilson, P., Darling, W.G., Jones, L. and Raines, M.** (2019) Groundwater–glacier meltwater interaction in proglacial aquifers. *Hydrol. Earth Syst. Sci.*, **23**, 4527–4539.
- Okko, M.** (1962) On the development of the first Salpausselkä, west of Lahti. Bulletin de la Commission Geologique de Finlande no. 202, 154p.
- Olanrewaju, J.N. and Wong, T.** (1984) Hydraulic conductivity, porosity, and particle size distribution of core samples of the upper glacial aquifer: laboratory observations, pp. 73–79. Long Island Geologists' Abstracts Collection [SBU][397].
- Oldenburg, D.W. and Li, Y.** (1999) Estimating depth of investigation in dc resistivity and IP surveys. *Geophysics*, **64**, 403–416.
- Orton, G.J. and Reading, H.G.** (1993) Variability of deltaic processes in terms of sediment supply, with particular emphasis on grain size. *Sedimentology*, **40**, 475–512.
- Osterloff, P., Al-Harthy, A., Penney, R., Spaak, P., Williams, G., Al-Zadjali, F., Jones, N., Knox, R., Stephenson, M.H., Oliver, G. and Al-Husseini, M.I.** (2004a) Depositional sequences of the gharif and khuff formations, subsurface interior Oman. In: *Carboniferous, Permian and Early Triassic Arabian Stratigraphy* (Ed. Al-Husseini, M.I.). GeoArabia Special Publications, **3**. Gulf PetroLink, Bahrain.
- Osterloff, P., Penney, R., Aitken, J., Clark, N. and Al-Husseini, M.I.** (2004b) Depositional sequences of the Al Khlata Formation, subsurface interior Oman GeoArabia. In: *Carboniferous, Permian and Early Triassic Arabian Stratigraphy* (Ed. Al-Husseini, M.I.). GeoArabiaSpecial Publications, **3**, 155. Gulf PetroLink, Bahrain.
- Ottesen, D., Dowdeswell, J.A., Rise, L. and Bugge, T.** (2012) Large-scale development of the mid-Norwegian shelf over the last three million years and potential for hydrocarbon reservoirs in glacial sediments. *Geol. Soc. London, Spec. Public.*, **368**(1), 53–73.
- Palacky, G.J.** (1988) 3. Resistivity Characteristics of Geologic Targets. In: *Electromagnetic Methods in Applied Geophysics*, Society of Exploration Geophysicists, pp. 52–129. Society of Exploration Geophysicists, Tulsa.
- Palmu, J.P.** (1999) *Sedimentary environment of the second salpausselkä ice marginal deposits in the Karkkila-Loppi area in southwestern Finland*. Geological Survey of Finland Report of investigation, **148**.
- Patton, H., Hubbard, A., Andreassen, K., Auriac, A., Whitehouse, P.L., Stroeven, A.P., Shackleton, C., Winsborrow, M., Heyman, J. and Hall, A.M.** (2017) Deglaciation of the Eurasian ice sheet complex. *Quat. Sci. Rev.*, **169**, 148–172.
- Paulamäki, S., Paananen, M. and Elo, S.** (2002) *Structure and Geological Evolution of the Bedrock of Southern Satakunta, SW Finland*. Geological Survey of Finland, Helsinki.
- Paz, C., Alcalá, F.J., Carvalho, J.M. and Ribeiro, L.** (2017) Current uses of ground penetrating radar in groundwater-dependent ecosystems research. *Sci. Total Environ.*, **595**, 868–885.
- Pisarska-Jamrozy, M. and Weckwerth, P.** (2013) Soft-sediment deformation structures in a Pleistocene glaciolacustrine delta and their implications for the recognition of subenvironments in delta deposits. *Sedimentology*, **60**, 637–665.
- Pisarska-Jamrozy, M. and Zieliński, T.** (2014) Pleistocene sandur rhythms, cycles and megacycles: Interpretation of depositional scenarios and palaeoenvironmental conditions. *Boreas*, **43**, 330–348.
- Poeter, E. and Gaylord, D.R.** (1990) Influence of aquifer heterogeneity on contaminant transport at the Hanford site. *Groundwater*, **28**, 900–909.
- Postma, G.** (1990a) Depositional architecture and Facies of river and fan deltas: A synthesis. In: *Coarse-Grained Deltas* (Eds Colella, A. and Prior, D.B.), pp. 13–27. Blackwell Publishing Ltd., Oxford.
- Postma, G.** (1990b) An analysis of the variation in delta architecture. *Terra Nov.*, **2**, 124–130.
- Powell, R.D.** (1990) Glacimarine processes at grounding-line fans and their growth to ice-contact deltas. *Geol. Soc. London. Spec. Publ.*, **53**, 53–73.
- Pye, K.** (1993) Introduction: The nature and significance of aeolian sedimentary systems. *Geol. Soc. Spec. Publ.*, **72**, 1–4.
- Pye, K. and Lancaster, N.** (1993) *Aeolian Sediments: Ancient and Modern*. Blackwell Scientific Publications, Hoboken, 167 pp.
- Ravier, E. and Buoncristiani, J.F.** (2017) Glaciohydrogeology. In: *Past Glacial Environments* (Eds Menzies, J. and van der Meer, J.J.M.), 2nd edn, pp. 431–466. Elsevier Ltd, Amsterdam.
- Reinardy, B.T.I. and Lukas, S.** (2009) The sedimentary signature of ice-contact sedimentation and deformation at macro- and micro-scale: A case study from NW Scotland. *Sediment. Geol.*, **221**, 87–98.
- Rinterknecht, V.R., Clark, P.U., Raisbeck, G.M., Yiou, F., Brook, E.J., Tschudi, S. and Lunkka, J.P.** (2004) Cosmogenic ¹⁰Be dating of the Salpausselkä I Moraine in southwestern Finland. *Quat. Sci. Rev.*, **23**, 2283–2289.
- Rohais, S., Eschard, R. and Guillocheau, F.** (2008) Depositional model and stratigraphic architecture of rift climax Gilbert-type fan deltas (Gulf of Corinth, Greece). *Sediment. Geol.*, **210**, 132–145.
- Rose, P., Byerley, G., Vaughan, O., Cater, J., Rea, B.R., Spagnolo, M. and Archer, S.** (2016) Aviat: a Lower Pleistocene shallow gas hazard developed as a fuel gas supply for the Forties Field. *Geol. Soc. London. Pet. Geol. Conf. Ser.*, **8**, 485–505.

- Russell, H.A.J.** and **Arnott, R.W.C.** (2003) Hydraulic-jump and hyperconcentrated-flow deposits of a glacial subaqueous fan: Oak ridges Moraine, southern Ontario, Canada. *J. Sediment. Res.*, **73**, 887–905.
- Rust, B.R.** and **Romanelli, R.I.** (1975) Late Quaternary subaqueous Outwash Deposits Near Ottawa, Canada. In: *Glaciofluvial and Glaciolacustrine Sedimentation.*, pp. 177–192. SEPM (Society for Sedimentary Geology), Broken Arrow.
- Saarnisto, M.** and **Saarinén, T.** (2001) Deglaciation chronology of the Scandinavian Ice Sheet from the Lake Onega Basin to the Salpausselkä End Moraines. *Glob. Planet. Change*, **31**, 387–405.
- Salem, H.S.** (2001a) Determination of porosity, formation resistivity factor, Archie cementation factor, and pore geometry factor for a glacial aquifer. *Energy Sources*, **23**, 589–596.
- Salem, H.S.** (2001b) Determination of porosity, formation resistivity factor, archie cementation factor, and pore geometry factor for a glacial aquifer. *Energy Sources*, **23**, 589–596.
- Satter, A.** and **Iqbal, G.M.** (2016) Reservoir rock properties. In: *Reservoir Engineering* (Eds Satter, A. and Iqbal, G.M.), pp. 29–79. Amsterdam: Elsevier.
- Sauramo, M.** (1929) The Quaternary geology of Finland. *Geologiska Föreningen i Stockholm. Föreläsningar*, **51** (4), 617–618.
- Sauramo, M.** (1931) Zur Frage des Inneren Baus des Sapausselkä in Finnland. *Zeitschrift für Gletscherkd.*, **XIX**, 300–315.
- Schomacker, A.** and **Benediktsson, Í.Ö.** (2017) Supraglacial environments. In: *Past Glacial Environments* (Eds Menzies, J. and van der Meer, J.J.M), 2nd edn. Elsevier Ltd, Amsterdam, pp. 159–179.
- Shackleton, C., Patton, H., Hubbard, A., Winsborrow, M., Kingslake, J., Esteves, M., Andreassen, K. and Greenwood, S.L.** (2018) Subglacial water storage and drainage beneath the Fennoscandian and Barents Sea ice sheets. *Quat. Sci. Rev.*, **201**, 13–28.
- Slomka, J.M.** and **Eyles, C.H.** (2013) Characterizing heterogeneity in a glaciofluvial deposit using architectural elements, Limehouse, Ontario, Canada. *Can. J. Earth Sci.*, **50**, 911–929.
- Slomka, J.M.** and **Eyles, C.H.** (2015) Architectural-landsystem analysis of a modern glacial landscape, Sólheimajökull, southern Iceland. *Geomorphology*, **230**, 75–97.
- Spedding, N.** and **Evans, D.J.A.** (2002) Sediments and landforms at Kviárjökull, southeast Iceland: A reappraisal of the glaciated valley landsystem. *Sediment. Geol.*, **149**, 21–42.
- Storrar, R.D., Ewertowski, M., Tomczyk, A.M., Barr, I.D., Livingstone, S.J., Ruffell, A., Stoker, B.J. and Evans, D.J.A.** (2019) Equifinality and preservation potential of complex eskers. *Boreas*, **49**, 211–231.
- Storrar, R.D., Stokes, C.R. and Evans, D.J.A.** (2014) Morphometry and pattern of a large sample (%3e20,000) of Canadian eskers and implications for sub-glacial drainage beneath ice sheets. *Quat. Sci. Rev.*, **105**, 1–25.
- Stroeven, A.P., Hättestrand, C., Kleman, J., Heyman, J., Fabel, D., Fredin, O., Goodfellow, B.W., Harbor, J.M., Jansen, J.D., Olsen, L., Caffee, M.W., Fink, D., Lundqvist, J., Rosqvist, G.C., Strömberg, B. and Jansson, K.N.** (2016) Deglaciation of Fennoscandia. *Quat. Sci. Rev.*, **147**, 91–121.
- Sutinen, R.** (1992) Glacial deposits, their electrical properties and surveying by image interpretation and ground penetrating radar. *Bull. Geol. Surv. Finl.*, **359**, 1–123.
- Thomas, G.S.P.** and **Chiverrell, R.C.** (2006) A model of subaqueous sedimentation at the margin of the Late Midlandian Irish Ice Sheet, Connemara, Ireland, and its implications for regionally high isostatic sea-levels. *Quat. Sci. Rev.*, **25**, 2868–2893.
- Van Loon, A.J.T.** and **Pisarska-Jamrozy, M.** (2014) Sedimentological evidence of Pleistocene earthquakes in NW Poland induced by glacio-isostatic rebound. *Sediment. Geol.*, **300**, 1–10.
- Virtasalo, J.J., Schröder, J.F., Luoma, S., Majaniemi, J., Mursu, J. and Scholten, J.** (2019) Submarine groundwater discharge site in the First Salpausselkä ice-marginal formation, south Finland. *Solid Earth*, **10**, 405–423.
- Walker, M., Johnsen, S., Rasmussen, S.O., Popp, T., Steffensen, J.-P., Gibbard, P., Hoek, W., Lowe, J., Andrews, J., Björck, S., Cwynar, L.C., Hughen, K., Kershaw, P., Kromer, B., Litt, T., Lowe, D.J., Nakagawa, T., Newnham, R. and Schwander, J.** (2009) Formal definition and dating of the GSSP (Global Stratotype Section and Point) for the base of the Holocene using the Greenland NGRIP ice core, and selected auxiliary records. *J. Quat. Sci.*, **24**, 3–17.
- Westoby, M.J., Glasser, N.F., Brasington, J., Hambrey, M.J., Quincey, D.J. and Reynolds, J.M.** (2014) Modelling outburst floods from moraine-dammed glacial lakes. *Earth-Science Rev.*, **134**, 137–159.
- Wingfield, R.** (1990) The origin of major incisions within the Pleistocene deposits of the North Sea. *Mar. Geol.*, **91**, 31–52.
- Winsemann, J., Alho, P., Laamanen, L., Goseberg, N., Lang, J. and Klostermann, J.** (2016) Flow dynamics, sedimentation and erosion of glacial lake outburst floods along the Middle Pleistocene Scandinavian Ice Sheet (northern central Europe). *Boreas*, **45**, 260–283.
- Winsemann, J., Brandes, C. and Polom, U.** (2011) Response of a proglacial delta to rapid high-amplitude lake-level change: an integration of outcrop data and high-resolution shear wave seismics. *Basin Res.*, **23**, 22–52.
- Winsemann, J., Hornung, J.J., Meisen, J., Aspöhn, U., Polom, U., Brandes, C., Bußmann, M. and Weber, C.** (2009) Anatomy of a subaqueous ice-contact fan and delta complex, Middle Pleistocene, North-west Germany. *Sedimentology*, **56**, 1041–1076.
- Winsemann, J., Lang, J., Polom, U., Loewer, M., Igel, J., Pollok, L. and Brandes, C.** (2018) Ice-marginal forced regressive deltas in glacial lake basins: geomorphology, facies variability and large-scale depositional architecture. *Boreas*, **47**, 973–1002.
- Zecchin, M., Catuneanu, O. and Rebesco, M.** (2015) High-resolution sequence stratigraphy of clastic shelves IV: High-latitude settings. *Mar. Pet. Geol.*, **68**, 427–437.
- Zieliński, T. and van Loon, A.J.J.** (1998) Subaerial terminoglacial fans I: A semi-quantitative sedimentological analysis of the proximal environment. *Geol. en Mijnbouw/Netherlands J. Geosci.*, **77**, 1–15.
- Zieliński, T. and van Loon, A.J.J.** (1999) Subaerial terminoglacial fans II: A semi-quantitative sedimentological analysis of the middle and distal environments. *Geol. en Mijnb.*, **78**, 73–85.
- Zieliński, T. and van Loon, A.J.** (2000) Subaerial terminoglacial fans III: overview of sedimentary characteristics and depositional model. *Netherlands. J. Geosci. - Geol. en Mijnb.*, **79**, 93–107.

- Zielinski, T. and Van Loon, A.J. (2003) Pleistocene sandur deposits represent braidplains, not alluvial fans. *Boreas*, **32**, 590–611.
- Zolitschka, B., Francus, P., Ojala, A.E.K. and Schimmelmann, A. (2015) Varves in lake sediments - a review. *Quat. Sci. Rev.*, **117**, 1–41.

Manuscript received 28 January 2021; revision accepted 8 April 2021

Supporting Information

Additional information may be found in the online version of this article:

Figure S1. Sedimentary facies identified in studied sections. See Table 1 for a detailed description.

Figure S2. Radar facies identified from GPR profiles.

Figure S3. GPR profiles GPR1 GPR2, GPR3, GPR4, GPR6, GPR7, GPR10, GPR11, GPR12, GPR13 with interpretations.

Figure S4. Electrical resistivity tomography profile ERT1.

Figure S5. Electrical resistivity tomography profile ERT 2.

Table S1. Details of geophysical methods.

Table S2. Criteria for geophysical data interpretation.